Studying the Phase Diagram of QCD Matter at RHIC

A STAR white paper summarizing the the current understanding and describing future plans

28 March 2014

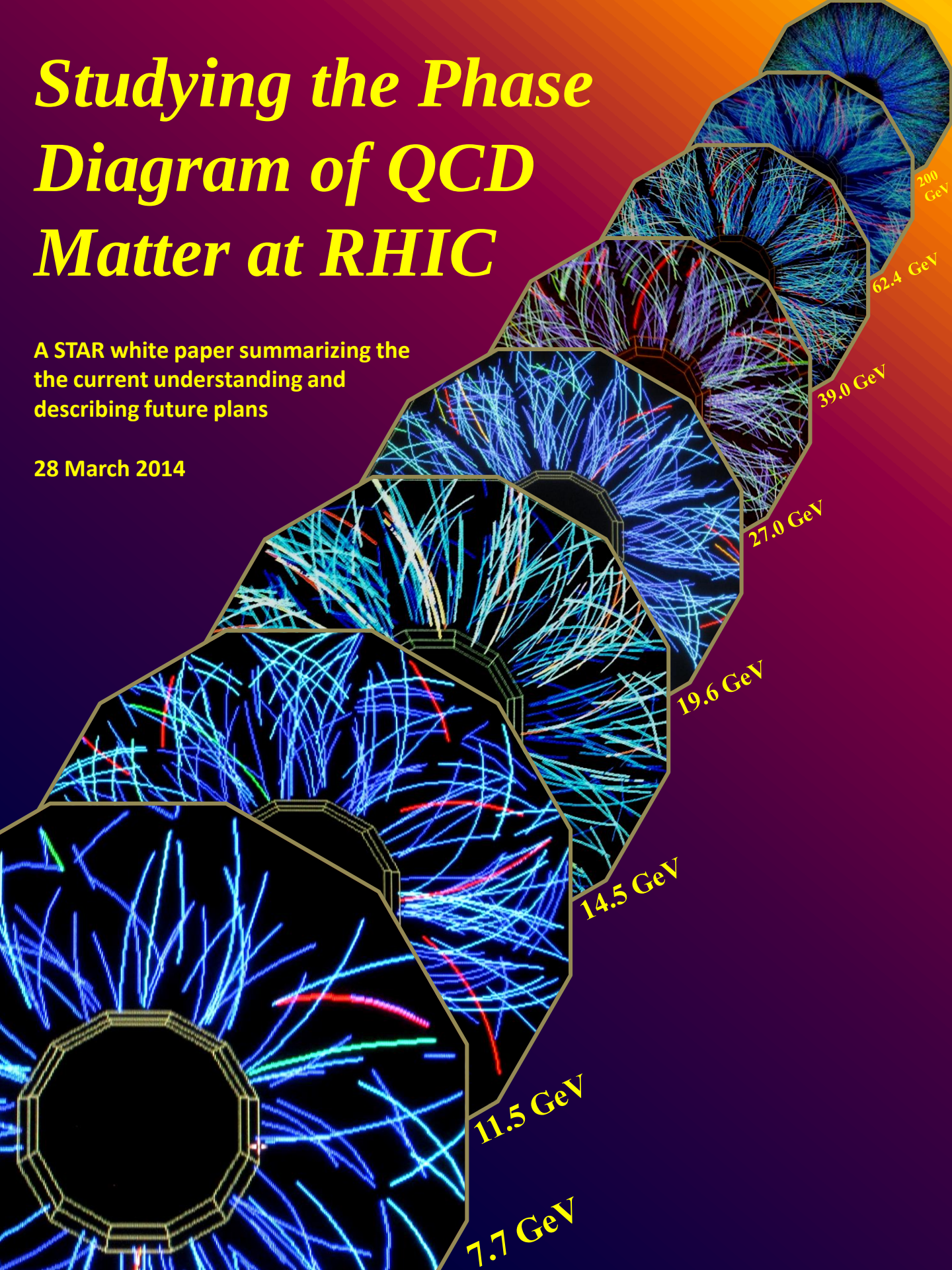

Executive Summary

The STAR Collaboration proposes a second phase of the Beam Energy Scan program at RHIC (BES Phase-II) to refine our understanding of the phase structure of QCD matter. The proposal is for two years (2018 and 2019) of dedicated low energy running at RHIC to make high precision measurements of the observables that have been found to be sensitive to the phase structure of QCD matter in the first phase of the program. The key points of this document are:

- The first phase of the Beam Energy Scan program (BES-I) plus the top energy at RHIC has allowed access to region of the QCD phase diagram covering a range of baryon chemical potential ($\mu_{\rm B}$) from 20 to 420 MeV corresponding to Au+Au collision energies from $\sqrt{s_{NN}}$ = 200 to 7.7 GeV, respectively. Results from BES-I have further confirmed the evidence for the quark-gluon plasma (QGP) discovery at the top RHIC energy $\sqrt{s_{NN}}$ = 200 GeV. The results of the search for the critical point and the first-order phase boundary have narrowed the region of interest to collision energies below $\sqrt{s_{\rm NN}}$ = 20 GeV. Current lattice QCD calculations suggest that key features of the phase diagram like the critical point and the first-order phase transition lie within the $\mu_{\rm B}$ reach of the RHIC BES program.
- The BES-I program has provided new information with measurements (e.g azimuthal anisotropy of produced particles and dilepton mass distributions) made at varying baryon density. The lowest beam energies in the BES-I are expected to correspond to the matter with the highest baryon density at freeze-out. Further, several measurements in BES-I coherently indicate that the role of partonic (hadronic) interactions increases (decreases) with beam energy.
- The proposed upgrades to the collider will increase the luminosity for future low energy runs by a factor of four to fifteen, depending on beam energy. The upgrades to the STAR detector system will significantly improve the quality of the measurements. The BES Phase-II program, with these upgrades, will allow for high-statistics measurements, with an extended kinematic range in rapidity and transverse momentum, using sensitive observables, to unfold the structure of the QCD phase diagram.

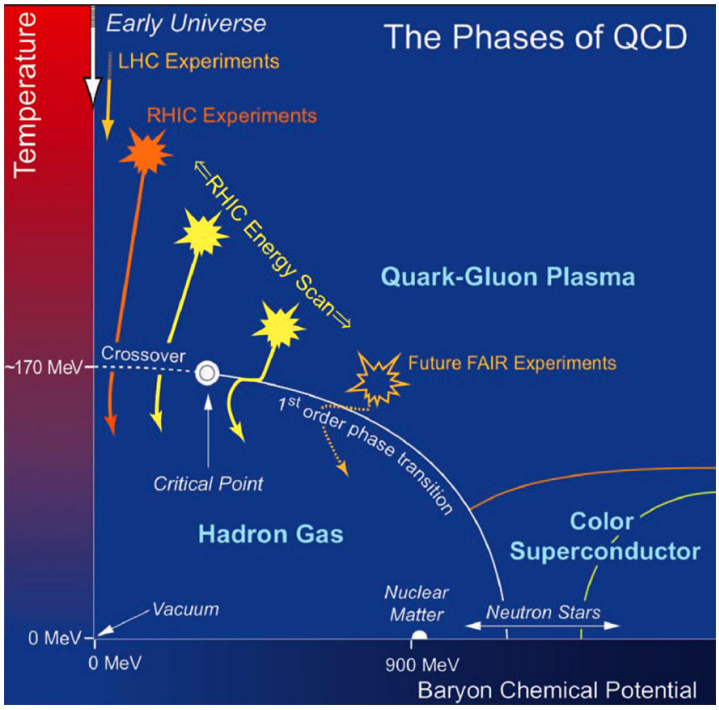

Figure 1. A conjectured QCD phase diagram with boundaries that define various states of QCD matter.

1. Introduction

A major goal of high-energy nuclear collisions is to determine the phase diagram for matter that interacts via the strong nuclear force. In contrast to the countless, very distinct phase diagrams found in condensed matter physics, the phase diagram probed in heavy-ion collisions is a unique and fundamental feature of Quantum Chromodynamics (QCD). The most experimentally accessible way to characterize the QCD phase diagram [1] is in the plane of temperature (T) and the baryon chemical potential (μ_B) [2]. Figure 1 is a conjectured version with μ_B on the horizontal axis. It shows a schematic layout of the phases, along with hypothesized indications of the regions crossed in the early stages of nuclear collisions at various beam energies.

Hadronic matter is a state in which the fundamental constituents, quarks and gluons, are confined in composite particles, namely baryons and mesons. At high energy densities, QCD predicts a phase transition from hadronic matter to a state of deconfined, partonic matter called the quark-gluon plasma (QGP) [3, 4]. The QCD vacuum is characterized by many non-vanishing condensates such as the gluon condensate and the quark condensate. These condensates characterize the confined phase of quark matter. In hot and dense QCD matter, the hadrons are melted into their constituent quarks, and the strong interaction becomes the dominant feature of the physics. In addition to the confined-deconfined transition, a chiral phase transition is postulated. Since the intrinsic scale of QCD is $\Lambda_{\rm QCD} \sim 200$ MeV, it is conceivable that the chiral phase transition line extends from around $T \sim \Lambda_{\rm QCD}$ at low baryon

number density (n_B) to around $n_B \sim \Lambda_{\rm QCD}^3 \sim 1/{\rm fm}^{-3}$ at low T.

Lattice QCD calculations have established that the quark-hadron transition to be a crossover transition at the temperature around 154 MeV for μ_B = 0 [5, 6, 7, 8, 9]. On the other hand, QCD-based models predict a first-order phase transition and the existence of an end point or critical point at high μ_B [10, 11]. However, the locations of the phase boundary and the critical point in this framework depend on model assumptions [12]. Experimentally, laboratory studies of relativistic heavy-ion collisions can provide us only with a chance to make microscopic, short-lived, and anisotropic volumes of QCD matter. We access properties of the matter by studying the evolution of these systems as they expand, cool, and possibly undergo phase transitions. Experiments at the Relativistic Heavy Ion Collider (RHIC) and the Large Hadron Collider (LHC) have provided compelling evidence of the formation of a deconfined state of quarks and gluons (QGP) for matter close to $\mu_B = 0$. The existence of a critical point and first-order phase transition at higher μ_B remains to be confirmed experimentally.

In order to study experimentally the QCD phase structure as a function of T and μ_B, a scan of beam energies is employed. Several collision energies are used to create systems which form at a variety of initial coordinates in T and μ_B. As the systems evolve, the adiabatic expansion is governed by the QGP equation of state. Therefore, as the system expands, T is reduced and μ_B, which is a measure of the excess of quarks relative to antiquarks, may also evolve. The excess of quarks is due to the valence quarks of the stopped participant baryons from the two colliding nuclei. By creating systems with a range of initial conditions, it is hoped that the different reaction trajectories cross different features in the phase diagram. Heavy ion collision programs at the Alternating Gradient Synchrotron (AGS) and the Super Proton Synchrotron (SPS) launched the study of some of the physics topics targeted by the RHIC BES. For example, the onset of deconfinement has been claimed at the SPS [13]. Although the fixed target experiments benefited from relatively high collision rates, analyses of data from these early programs are complicated, as the experimental acceptances and particle identification vary with beam energy. Neither program could reach the high beam energies where the QGP is cleanly established. Phase-I of a Beam Energy Scan (BES-I) program at RHIC addressed these issues and began taking data in the year 2010 [14, 15].

The purpose of the BES-I program was three-fold: (a) to search for threshold energies for the QGP signatures that have already been established at the top RHIC energies, thereby corroborating the past QGP discoveries; (b) to search for signatures of a first-order phase transition; and (c) to search for a QGP/hadron gas critical point. Data were collected during 2010 and 2011 at 6 energies. Data from a final BES-I energy point at 14.5 GeV were collected in February and March of 2014. The details of the BES-I program are listed in Table 1.

Here we report a summary of selected experimental results from BES-I. During the course of the presentation of results, we also discuss the current theoretical status. For some of the results from BES-I, as discussed below (Section 2), the strength of the conclusions is limited by the uncertainty in the measurements. More definitive conclusions will be possible after a second phase of the program (BES Phase-II). In this second phase, we propose to concentrate on collecting high event statistics at the lower-energy end of the BES-I range

Table 1. An overview of Beam Energy Scan Phase-I. The μ_B values are estimated from the systematics of central collisions in Ref. [16]. The 200 GeV is also listed in the table as a reference.

Beam Energy (in GeV)	Baryon Chemical Potential (in MeV)	Year of Data Taking	Event Statistics (Millions)	Beam Time (Weeks)
200	20	2010	350	11
62.4	70	2010	67	1.5
39	115	2010	130	2.0
27	155	2011	70	1.0
19.6	205	2011	36	1.5
14.5	260	2014	20	3.0
11.5	315	2010	12	2.0
7.7	420	2010	4	4.0

($\sqrt{s_{NN}} < 20$ GeV). Details of the BES Phase-II proposal will be discussed in Section 3. In Section 3, we also comment on the possibility of an increase in luminosity for the lower beam energies through electron cooling at RHIC, and discuss briefly our proposed detector upgrades to enhance the scientific/technical quality of the various results. Finally, in Section 4, we summarize the scientific part of the RHIC BES program.

2. Review of BES-I Results and Theory Status

2.1. Region of the Phase Diagram Accessed in BES-I

Experimentally, different regions of the phase diagram are accessed by changing the beam energy. Both initial T and $\mu_{\rm B}$ vary as functions of the center-of-mass energy ($\sqrt{s_{\rm NN}}$) [17]. This is the strategy adopted in the BES program at RHIC [14, 15]. It is possible to estimate the T and $\mu_{\rm B}$ regions of the phase diagram accessed for a given collision energy through the study of the hadron spectra. These spectra reflect the properties of the bulk matter at kinetic freeze-out, after elastic collisions among the hadrons have ceased. Information on the earlier stages can be deduced from the integrated yields of the different hadron species, which change only via inelastic collisions. The point in time at which these inelastic collisions cease is referred to as chemical freeze-out, which takes place before kinetic freeze-out. In the BES-I program at RHIC, almost all species of hadrons in the light and strange quark sectors, including $\pi^{\pm}$, $K^{\pm}(K^0_S)$, $p(\bar{p})$, ϕ, Λ, Ξ, and Ω have been detected and yields were measured as a function of collision centrality. As an example, Fig. 2 shows a representative plot of the invariant yields of π^+, K^+, K^0_S, ϕ, p, Λ and Ξ^- as a function of m_T - m, where $m_T = \sqrt{m^2 + p_T^2}$ is the transverse mass, m is the rest mass of the hadron and p_T the transverse momentum. The results are shown for various collision centralities in Au+Au collisions at $\sqrt{s_{NN}}$ = 11.5 GeV.

Within a statistical model which assumes thermodynamic equilibrium, the particle yields at chemical freeze-out in a system of volume V can be given by

$$N_i/V = \frac{g_i}{(2\pi)^3}\gamma_S^{S_i}\int \frac{1}{\exp\left(\frac{E_i-\mu_B B_i-\mu_S S_i}{T_{\rm ch}}\right)\pm 1} d^3p\,, \qquad (1)$$

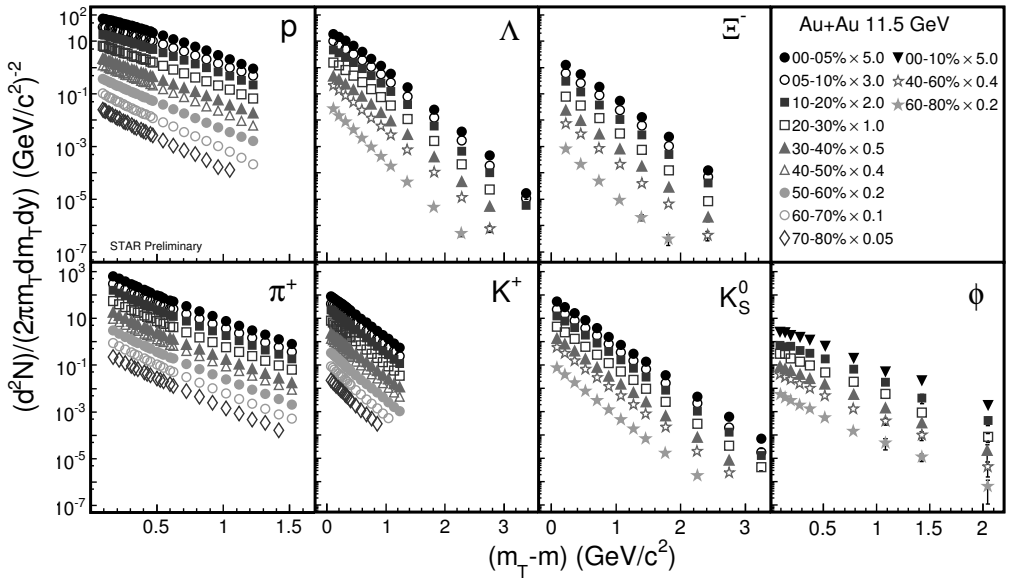

Figure 2. Invariant yields versus m_T - m of hadrons produced in Au+Au collisions at various collision centralities at $\sqrt{s_{NN}}$ = 11.5 GeV.

where N_i is the abundance of particle species i, g_i is the spin degeneracy, B_i and S_i are the baryon number and strangeness number, respectively, E_i is the particle energy, and the integral is taken over all momentum space [18]. The model parameters are the chemical freeze-out temperature ($T_{\rm ch}$), the baryon ($\mu_{\rm B}$) and strangeness (μ_S) chemical potentials, and the *ad hoc* strangeness suppression factor (γ_S). Measured particle yields (obtained by integrating the distributions in Fig. 2 over p_T) have been used to estimate the values of $T_{\rm ch}$ and $\mu_{\rm B}$ at chemical freeze-out, see Figure 3(a), using the statistical model THERMUS [19] and assuming that the system can be represented by a Grand Canonical ensemble.

The figure shows that RHIC programs, the top energy plus the BES-I, cover the μ_B region from $\sim$ 20 MeV ($\sqrt{s_{NN}}$ = 200 GeV) to $\sim$ 420 MeV ($\sqrt{s_{NN}}$ = 7.7 GeV), which is a larger range than at any other heavy-ion facility. The yellow band shows empirical $T_{\rm ch}$ versus $\mu_{\rm B}$ trends based on data obtained prior to the BES-I program using statistical models in the literature [16, 21].

The graph in Fig. 3(a) shows only a single point at chemical freeze-out in the system's expansion trajectory in the T vs. μ_B plane. The starting point of each trajectory is governed by the primordial conditions prevailing during the early equilibration phase. The evolution of the system is then influenced by the equation-of-state (EOS) as the system expands and cools until it reaches chemical freeze-out. In addition, The BES-I program provided measurements of the centrality dependence of the freeze-out parameters [22, 23]. Measurements of the centrality dependence have not previously been available in heavy-ion collisions and could be used to constrain the expansion dynamics. In BES Phase-II, a systematic measurement of the yields of a variety of produced hadrons versus rapidity, centrality, and beam energy will address

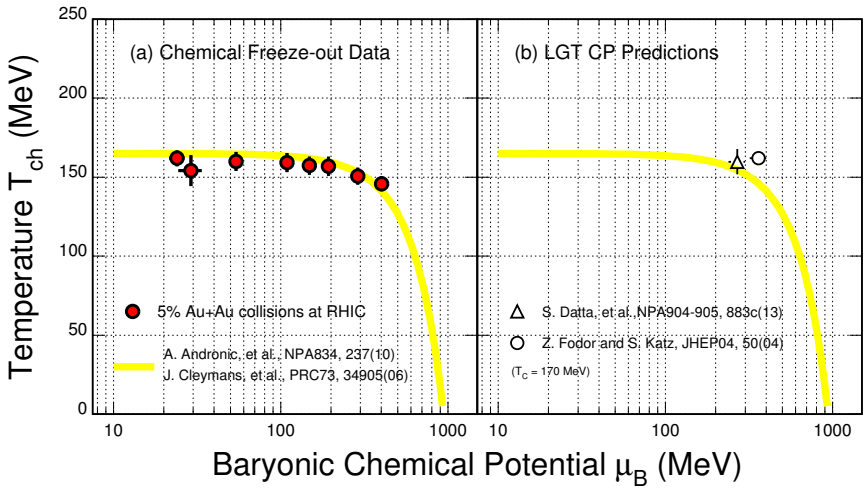

Figure 3. (a) Chemical freeze-out temperature ($T_{\rm ch}$) versus baryonic chemical potential ($\mu_{\rm B}$) obtained from a statistical model [20, 16] fit to yields of hadrons produced in 0-5% central Au+Au collisions at RHIC. The yellow bands are the empirical results from fitting experimental data acquired prior to the BES-I program by a statistical model. (b) The positions of the QCD critical point from two different lattice gauge theory calculations in the $T_{\rm ch}$ versus $\mu_{\rm B}$ plane are shown.

questions about the evolution of the hadron yields between the initial hadronization and the final thermal equilibrium [24] and about the possibility of successive hadronization [25]. This could lead to further development, understanding, and refinement of the statistical models. Recently, the possibility of extracting freeze-out properties by comparing the higher moments of multiplicity distributions of conserved numbers (net-charge and net-baryons) to QCD calculations of high order susceptibilities on the lattice has been proposed [26, 27]. This has been possible due to the construction of proper observables that allow for comparison between experiment and QCD calculations [28, 29].

Two estimates of the QCD critical point from lattice gauge theory calculations [30, 31] in the $T-\mu_{\rm B}$ plane taking $T_{\rm c}$ = 170 MeV are shown in Fig. 3(b). Based on these current estimates of the critical point from QCD calculations, we observe that the RHIC BES-I program scanned from energies for which the matter expands and cools through a crossover transition down to those which could contain key features of the phase diagram of QCD matter; specifically, the detailed study of the energy range from 7.7 to 19.6 GeV proposed in BES Phase-II is well suited to identify the critical point and the first-order phase transition boundary.

The transverse momentum distributions of the different particles contain two components, one random and one collective. The random component can be identified as the one that depends on the temperature of the system at kinetic freeze-out ($T_{\rm kin}$). The collective component, which arises from the matter density gradient from the center to the boundary of the fireball created in high-energy nuclear collisions, is generated by collective flow in the transverse direction and is characterized by its velocity ($\langle\beta\rangle$), also called the radial flow.

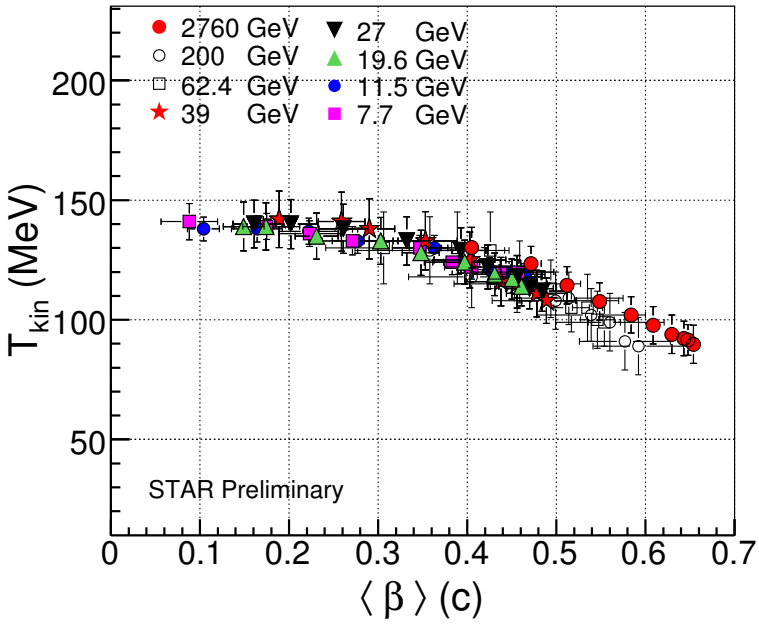

Figure 4. Kinetic freeze-out temperature ($T_{\rm kin}$) versus the average collective flow in the transverse direction ($\langle\beta\rangle$) in high energy heavy-ion collisions for different collision centralities. At each collision energy, the data points with lower $\langle\beta\rangle$ values correspond to peripheral collisions and those with the larger $\langle\beta\rangle$ values correspond to central collisions.

Assuming that the system attains thermal equilibrium, the blast-wave formulation [32] can be used to extract $T_{\rm kin}$ and $\langle\beta\rangle$. The $T_{\rm kin}$ versus $\langle\beta\rangle$ values obtained from the simultaneous fits to the $m_T - m$ distributions of π, K, and p (as shown in the representative plot in Fig. 2) at midrapidity at RHIC for various collision energies are shown in Fig. 4. Also shown are the corresponding results from Pb+Pb collisions at $\sqrt{s_{NN}}$ = 2.76 TeV from ALICE at the LHC [33]. The $T_{\rm kin}$ values in central collisions are lower than the corresponding values for $T_{\rm ch}$ (shown in Fig. 3) although the difference decreases at lower beam energies. At all the beam energies studied (BES-I, 200 GeV, and LHC [33]), there is an anti-correlation between $T_{\rm kin}$ and $\langle\beta\rangle$. This shows that peripheral collisions have a higher value of temperature (freeze-out earlier) and less collectivity is developed compared to central collisions (freeze-out later) [34].

2.2. Search for the Critical Point

Thermodynamic principles suggest that there should be a critical point in QCD matter where the first-order phase transition ends and the transition becomes a crossover [5, 9], at which point the phase boundaries effectively cease to exist. The characteristic experimental signature of the QCD critical point is large fluctuations in event-by-event multiplicity distributions of conserved quantities like net-charge, net-baryon number, and net-strangeness. The variances of these distributions ($\langle(\delta N)^2\rangle$) are proportional to the square of the correlation length (ξ). It has been shown that higher moments ($\langle(\delta N)^3\rangle \sim \xi^{4.5}$ and $\langle(\delta N)^4\rangle \sim \xi^7$) have stronger

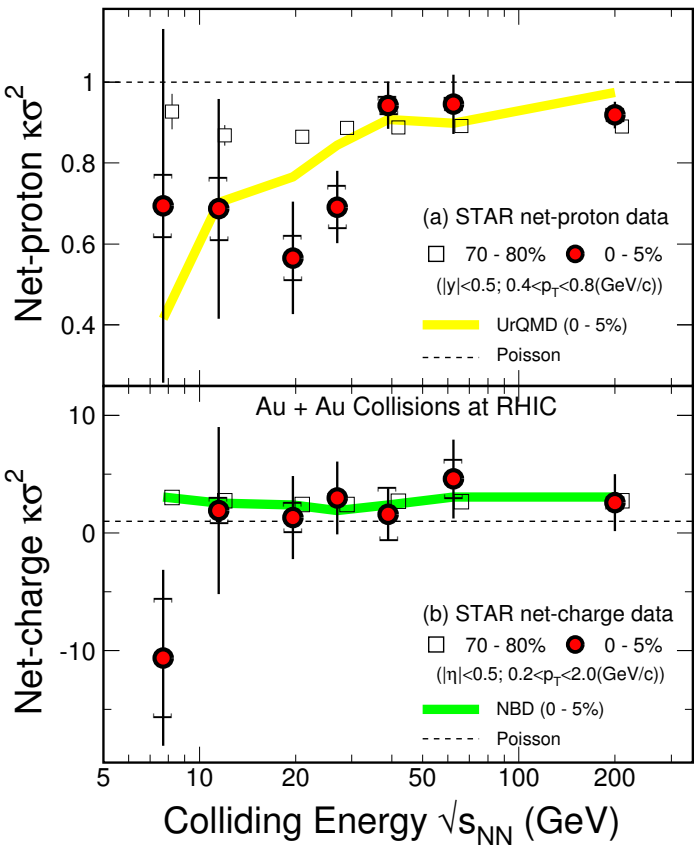

Figure 5. Collision energy dependence of net-proton (top panel) [40] and net-charge (bottom panel) [42] $\kappa\sigma^2$ from Au+Au collisions at RHIC. The red solid circles correspond to 0-5% central collisions and the open squares represent 70-80% peripheral collisions. The vertical error bars are statistical and the caps correspond to systematic errors. The yellow solid band in the top panel represents 0-5% central Au+Au collision results from UrQMD simulations and the green solid band in the bottom panel is the result where proton and anti-proton distributions follow independent negative binomial statistics. The dashed line in each panel represents the expectation from proton and anti-proton distributions following Poisson statistics.

dependences on ξ than the variance and might have higher sensitivity [35, 36, 37]. In addition, the moments are related to the susceptibilities (χ) [38] and hence a comparison can be directly made to QCD calculations [28, 29]. Motivated by these considerations, STAR has studied the kurtosis times the variance ($\kappa\sigma^2$) of net-proton (a proxy for net-baryon) and net-charge distributions to search for the critical point [39, 40]. In the absence of a critical point, the hadron resonance gas model [41] suggests that the $\kappa\sigma^2$ values will be close to unity and have a monotonic dependence on $\sqrt{s_{\rm NN}}$ [43]. However, because $\kappa\sigma^2$ is related to the ratio of conserved number susceptibilities in QCD models ($\kappa\sigma^2 = \frac{\chi^{(4)}}{\chi^{(2)}/T^2}$ [28]), it is expected to show a non-monotonic dependence on $\sqrt{s_{\rm NN}}$ close to the critical point.

Figure 5 shows the $\kappa\sigma^2$ for net-proton (top panel) [40] and net-charge (bottom panel) [42] distributions in Au+Au collisions at midrapidity as a function of colliding energy for two different collision centralities (0-5% and 70-80%). The net-proton $\kappa\sigma^2$ values for the 0-5% centrality selection at $\sqrt{s_{\rm NN}}$ = 19.6 and 27 GeV are observed to deviate from: (a) the values from 70-80% peripheral collisions which are expected to create small systems which are dominated by two-to-two processes and do not show significant bulk properties, (b) Poisson and hadron resonance gas expectation values, which would correspond to uncorrelated emission and are close to unity, and (c) transport-model-based UrQMD [44, 45] calculations, which represent the expectations of expanding drops of finite hadronic matter which does not experience a phase transition. A fourth baseline based on the model of independent production is under investigation and was briefly discussed in [40]. The conclusions which can be drawn from the net-charge $\kappa\sigma^2$ values are not clear because of the large uncertainties, which are driven by the larger value of the σ for the net-charge distributions. In addition, finite acceptance measurements of net-charge fluctuations are subject to the effect of resonance decay. Within the current statistical uncertainties, the data do not show a non-monotonic variation of the $\kappa\sigma^2$ of net-charge distributions as a function of $\sqrt{s_{\rm NN}}$. A possible non-monotonic variation of the $\kappa\sigma^2$ of the net-proton distribution is not excluded by the existing STAR data. High event statistics for collisions below 20 GeV in BES Phase-II will help clarify these issues.

2.3. Search for the First-order Phase Transition

A first-order phase transition is characterized by a discontinuity in one of the state variables. Lattice QCD predicts that there should be a discontinuity in the density below T_C [46]. A first-order phase transition is also characterized by an unstable coexistence region. This spinodal region will exhibit a change in compressibility, i.e., a softening of the EOS. A signature of this softening of the EOS is the pattern of directed flow (like its slope at midrapidity) versus beam energy [47, 48, 49]. Such flow patterns can be obtained by studying the Fourier expansion of the azimuthal angle (ϕ) distribution of produced particles with respect to the reaction plane angle (Ψ_R) [50]. Directed flow can be quantified by the first Fourier coefficient (v_1), while the elliptic flow is given by the second coefficient (v_2).

Another possible signature is a saturation of the average transverse momentum as a function of collision energy. It is based on the relation of temperature and entropy to the average transverse momentum and multiplicity, respectively. This signature was originally proposed by Van Hove in the context of proton-proton collisions [51]. It was argued that a plateau in the average transverse momentum beyond a certain value of multiplicity will indicate the onset of the formation of a mixed phase of QGP and hadrons, analogous to the plateau observed in the variation of temperature with entropy in a first-order phase transition scenario.

2.3.1. Directed Flow (v_1): Hydrodynamic calculations [47, 48, 49], including a three-fluid hydrodynamic model [48, 49] whose EOS incorporates a first-order phase transition, suggest

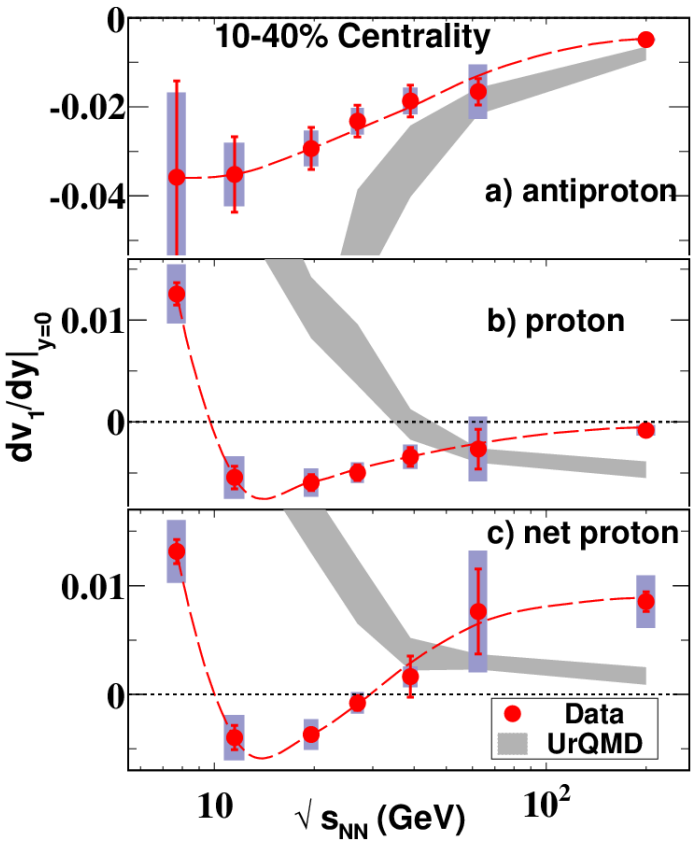

Figure 6. Directed flow slope (dv_1/dy) near mid-rapidity as a function of beam energy for intermediate-centrality (10-40%) Au+Au collisions. Panels (a), (b), and (c) report STAR's measurement for antiprotons, protons, and net-protons, respectively, along with corresponding calculations from the UrQMD hadronic transport model [44, 45] subject to the same cuts and fit conditions. The systematic uncertainties on the measurements are shown as shaded bars. The dashed curves are a smooth fit to guide the eye.

that the v_1 of net-baryons is sensitive to the early collision dynamics and can be used as a signature for the first-order phase transition. These calculations predict a non-monotonic variation of directed flow slope of baryons (or net-baryons) around midrapidity as a function of beam energy and feature a prominent minimum around $\sqrt{s_{NN}} = 4$ GeV and a double sign change in the v_1 slope, which is not seen in the same hydrodynamic model without a first-order phase transition. More up-to-date hydrodynamic calculations [52, 53] confirm this earlier prediction, but yield consistently larger v_1 magnitudes than observed by STAR in BES-I.

Figure 6(a) and (b) shows the beam energy dependence of the slope of directed flow at midrapidity (dv_1/dy) for antiprotons and protons, respectively [54]. For intermediate-centrality (10-40%) collisions, the proton slope decreases with energy and changes sign from positive to negative between 7.7 and 11.5 GeV, shows a minimum below 19.6 GeV, and remains small and negative up to 200 GeV. In contrast, the corresponding antiproton results always remain negative and approach the proton results at high beam energies. For comparison, the UrQMD hadronic transport model [44, 45], which has no phase transition

mechanism, does not show a non-monotonic behavior in the same energy range as the data.

The energy dependence of proton dv_1/dy involves an interplay between the proton v_1 associated with the baryon number transported from the initial state to mid-rapidities, and the proton v_1 from pair production near mid-rapidity. The importance of the second mechanism increases strongly with beam energy. A way to distinguish between the two mechanisms would be informative. We define the slope, $[dv_1/dy]_{\text{net-}p}$, based on expressing the rapidity dependence of directed flow for all protons as

$$[v_1(y)]_p = r(y)[v_1(y)]_{\bar{p}} + [1 - r(y)]\,[v_1(y)]_{\text{net-}p}\,,$$

where $r(y)$ is the observed rapidity dependence of the ratio of antiprotons to protons at each beam energy [54]. For reasons set out in Ref.[54], it is assumed that the antiproton directed flow is a proxy for the directed flow of produced protons. Therefore, $[dv_1/dy]_{\text{net-}p}$ isolates, as far as possible, the contributions from transported initial-state baryonic matter. Figure 6(c) shows that the $v_1(y)$ slope for net protons is negligibly different from protons below 19.6 GeV, but then rises, crosses zero between 27 GeV and 39 GeV, and remains positive up to 200 GeV. The UrQMD model [44, 45] shows a monotonic trend, with a positive slope at all energies.

An interpretation of the changing sign of the v_1 slope is that it reflects a change in EOS. At a given energy where the system undergoes a first-order parton-hadron phase transition, one expects the formation of a mixed phase, where the pressure gradient is small. The softest pressure could produce the observed minimum in the proton v_1 slope parameter. At higher energies, pair production is dominant at mid-rapidity and transported baryons have a relatively small influence. As there is no preferred direction for pair-produced hadrons, the slope parameter approaches zero. At lower beam energies, baryon transport is dominant, hence the slope parameter is positive. A mean-field model study shows that the energy-dependent baryon potential plays an important role in this region [55]. In the search for a first-order phase transition in the QCD phase diagram, the findings from the dv_1/dy analysis from the STAR BES-I strongly motivate further measurements at $\sqrt{s_{NN}} < 20$ GeV where the softest region of the EOS is suggested. To better understand the possible role and relevance of stopping in the existing data on proton and net-proton directed flow, new higher-statistics v_1 measurements as a function of centrality are needed.

2.3.2. Average Transverse Mass: Figure 7 (left panel) shows $\langle m_{\text{T}}\rangle - m$ for π and K in central Au+Au collisions as a function of the center-of-mass energy at RHIC [18]. The $\langle m_{\text{T}}\rangle - m$ can be interpreted as a measure of thermal excitation in the transverse direction (temperature), while dN/dy, which is a measure of the entropy (S), has been shown to be proportional to $\ln(\sqrt{s_{\text{NN}}})$. Also shown in Fig. 7 are results from Au+Au collisions at the AGS [56, 57, 58, 59, 60, 61], from Pb+Pb collisions at the SPS [62, 13] and LHC [33]. The $\langle m_{\text{T}}\rangle - m$ values increase with $\sqrt{s_{\text{NN}}}$ at AGS energies, stay independent of $\sqrt{s_{\text{NN}}}$ at SPS and RHIC BES-I energies, and then tend to rise again with increasing $\sqrt{s_{\text{NN}}}$ at the higher beam energies at RHIC [18] and at the LHC [33]. The results shown in the figure reflect the characteristic signature of a first-order phase transition, as first proposed by Van Hove [51].

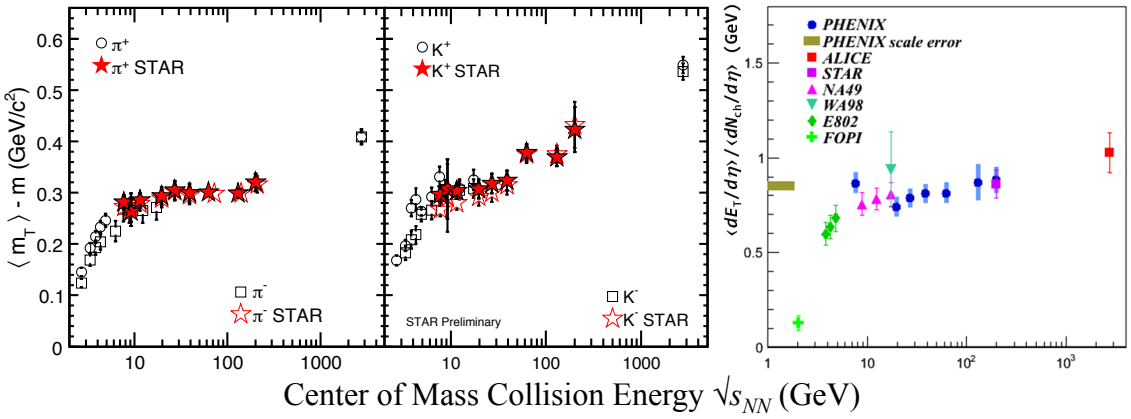

Figure 7. Left panel: Center-of-mass energy dependence of $\langle m_{\rm T}\rangle - m$ of π and K, in central Au+Au collisions at midrapidity at RHIC. Also shown are the corresponding results from experiments at the AGS [56, 57, 58, 59, 60, 61], SPS [62, 13], and LHC [33]. The errors shown are the quadrature sum of statistical and systematic uncertainties. Right panel: The average transverse energy, scaled by the charged particle multiplicity at mid-rapidity, as a function of collision energy observed by the PHENIX, ALICE, STAR, NA49, WA98, E802, and FOPI Collaborations [63].

For comparison to STAR's $\langle m_{\rm T}\rangle - m$, we show a compilation of $\langle dE_{\rm T}/d\eta\rangle/\langle dN_{\rm ch}/d\eta\rangle$ results prepared by the PHENIX collaboration [63] in Fig. 7 (right panel). As one can see in the figure, there is qualitative agreement between the saturation in $\langle E_{\rm T}\rangle$ (right panel) and $\langle m_{\rm T}\rangle - m$ (left panel), although the absolute values of $\langle E_{\rm T}\rangle$ are much larger.

2.4. Search for the Threshold of QGP Formation

Several distinct signatures of the formation of a new state of hot and dense matter, where relevant degrees of freedom are quarks and gluons, have been reported on the basis of data from top RHIC energy [34, 64, 65]. These include (i) the measurement of a large magnitude of the elliptic flow (close to that expected from ideal hydrodynamics in a system of deconfined quarks and gluons) for both light and strange-quark carrying hadrons, and the discovery of the number-of-constituent-quark ($n_{\rm Q}$) scaling of elliptic flow of identified hadrons [66, 67, 68, 69]; (ii) the observation of the phenomenon of jet quenching through the measurement of the nuclear modification factor of produced hadrons at high transverse momentum [70, 71, 72, 73], and (iii) the observation of dynamical charge correlations with respect to the reaction plane [74, 75]. In this section, we discuss how the BES-I results corroborate the findings of the formation of QGP at the top RHIC energy.

2.4.1. Elliptic Flow: The study of collective flow in relativistic nuclear collisions could provide insights into the EOS of the matter created during heavy-ion collisions. As discussed earlier, there are two types of azimuthal anisotropy that are commonly studied in heavy-ion collisions, directed flow (v_1) and elliptic flow (v_2). In this subsection, we concentrate on

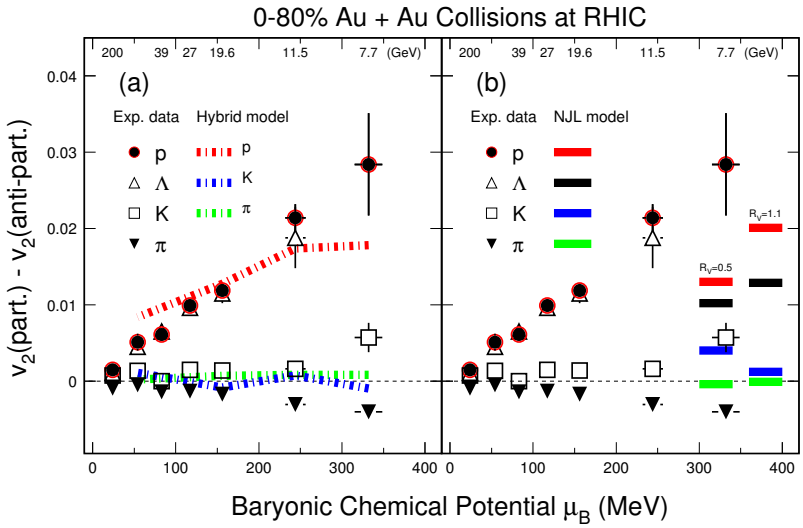

Figure 8. The measured difference in integrated v_2 between particles and their corresponding antiparticles: pions (filled triangles), kaons (open squares), Λs (open triangles), and protons (filled circles), all shown as a function of baryonic chemical potential and collision energy for 0–80% Au+Au collisions [82, 83]. Only statistical error bars are shown. Panels (a) and (b) show the comparison with model calculations from Refs. [85] and [86, 87], respectively.

v_2. The v_2 coefficient has proven to be one of the most discussed probes of the dynamics in Au+Au collisions at RHIC [76, 77, 78, 79, 80].

Figure 8 shows the first experimental observation of the difference in the integrated v_2 at midrapidity between particles and their corresponding antiparticles for pions, kaons, Λs, and protons, shown as a function of the baryonic chemical potential [81] and center-of-mass energy for minimum-bias (0–80%) Au+Au collisions [82, 83]. The v_2 difference is positive for all the hadrons studied, except for pions. The difference in v_2 is almost linearly proportional to the value of the baryon chemical potential. This indicates a connection between the v_2 differences and the net-baryon density at chemical freeze-out.

The negative value of the v_2 difference for pions has been predicted [84] to be due to the interplay between the strong external magnetic field and the density wave of both electric and chiral charges, in semi-central high-energy nuclear collisions. On the other hand, several studies in the literature [85, 86, 87, 88] attempt to explain the observed differences with hadronic interactions at lower beam energies. In Fig. 8(a), dashed lines represent model results from a hybrid calculation featuring Boltzmann transport with an intermediate hydrodynamic stage [85]. This approach can reproduce the observed v_2 difference between baryons and antibaryons. It reproduces the small value of the v_2 difference for pions, however, the sign of the observable in the model is opposite to that of the observations. The authors of Ref. [85] have argued that the BES-I data show that it is important to properly treat strangeness production and isospin conservation.

Figure 8(b) shows the results from Nambu-Jona-Lasinio (NJL) mean-field model calculations with two values of the ratio (R_v) of the vector coupling to the scalar-pseudoscalar

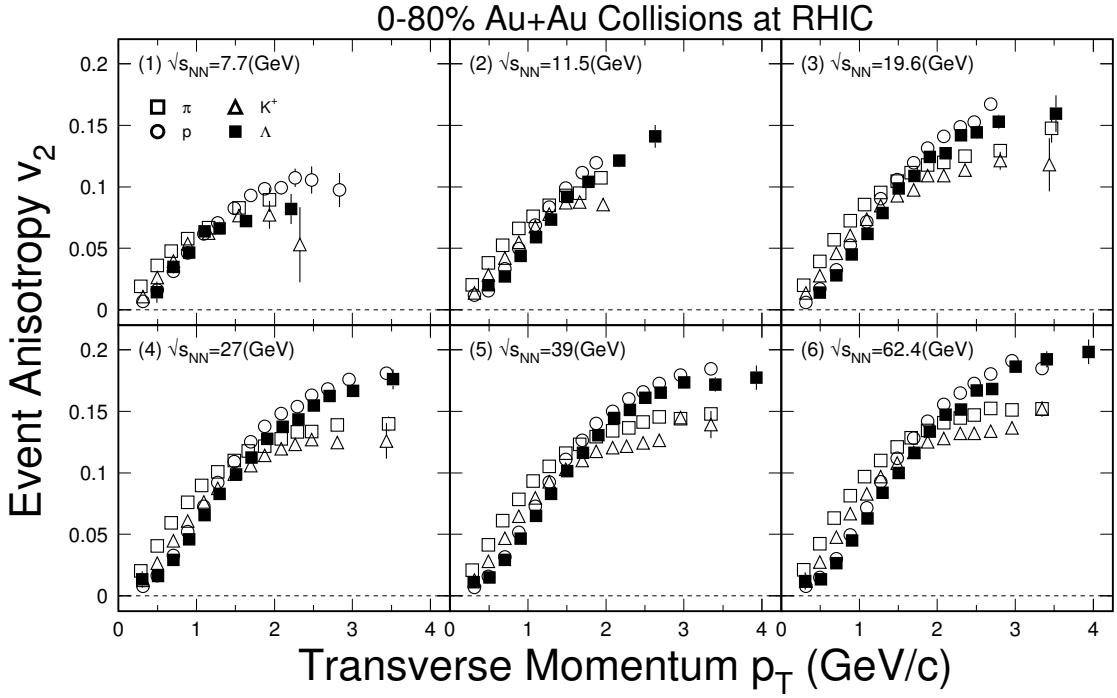

Figure 9. The experimental results of the identified hadron anisotropy parameter v_2 from minimum bias (0–80%) Au+Au collisions at six collision energies [82, 83].

coupling [86, 87] that are compared to the data for $\sqrt{s_{\rm NN}}$ = 7.7 GeV. The model reproduces the correct order of the v_2 splitting but misses the values of the v_2 differences quantitatively. The authors have pointed out that the magnitude of the v_2 splitting is sensitive to the vector coupling which, in turn, could be baryon-density dependent. Note that the vector coupling is close to zero at vanishing net-baryon density. According to Ref. [89], such baryon-density dependent vector interactions may affect the location of the critical point in the QCD phase diagram. The authors of Ref. [88] have pointed out the importance of the transport of baryon charge in high-energy nuclear collisions as a possible explanation of the experimental data.

Figure 9 shows the v_2 of identified hadrons (π^+, K^+, p, and Λ) as a function of transverse momentum for minimum-bias (0–80%) Au+Au collisions at RHIC BES-I energies [82, 83]. As was observed at the top RHIC energy, below a $p_{\rm T}$ of 2 GeV/c, the $v_2(p_{\rm T})$ values are hadron-mass ordered. Lighter hadrons have a larger v_2 compared to heavier hadrons. Above $p_{\rm T}$ = 2 GeV/c, the characteristic baryon-meson splitting of $v_2(p_{\rm T})$ is seen for $\sqrt{s_{\rm NN}}$ = 27, 39, and 62.4 GeV collisions, as was observed at $\sqrt{s_{\rm NN}}$ = 200 GeV [80]. Such a splitting was a basis of the claim of recombination being a process of hadronization [90, 91, 92], which in turn is connected to the existence of partonic collectivity, and the formation of a deconfined phase in high energy heavy-ion collisions. At $\sqrt{s_{\rm NN}}$ = 19.6 GeV, the baryon-meson splitting appears to be reduced, thereby suggesting a reduced contribution to the collectivity. The limited range of $p_{\rm T}$ allowed by the event statistics at $\sqrt{s_{\rm NN}}$ = 7.7 and 11.5 GeV makes conclusions difficult for these energies.

Figure 10 shows v_2 scaled by the number of constituent quarks ($n_{\rm Q}$) for identified

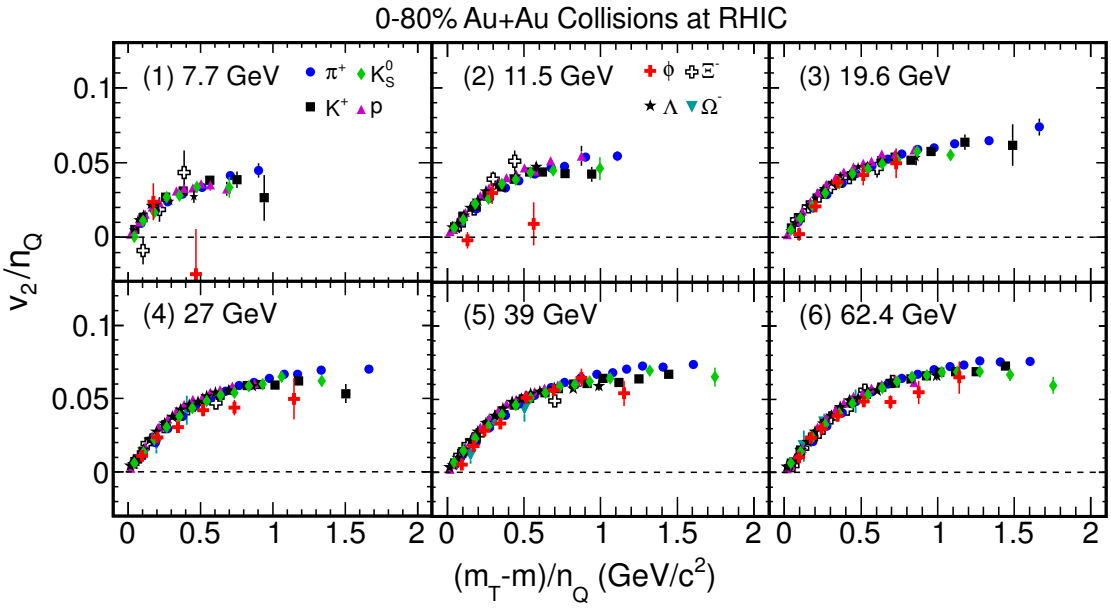

Figure 10. The number-of-constituent-quark scaled anisotropy parameter v_2, for identified hadrons from minimum-bias (0–80%) Au+Au collisions at six collision energies [82, 83]. Here n_Q stands for the number of constituent quarks.

hadrons, as a function of $n_{\rm Q}$-scaled $m_{\rm T} - m$ for 0-80% Au+Au collisions at $\sqrt{s_{NN}}$ = 7.7, 11.5, 19.6, 27, 39, and 62.4 GeV [82, 83]. For the momentum range studied, the $n_{\rm Q}$ scaling is observed to be within $\sim 10\%$ for all the plotted beam energies [82, 83]. The major differences compared to the corresponding results at $\sqrt{s_{\rm NN}}$ = 200 GeV are as follows. (i) At the top RHIC energy, all particles and antiparticles together follow the $n_{\rm Q}$ scaling in v_2. This conclusion is confirmed by the PHENIX analysis of v_2 at 39 and 62.4 GeV [93]. However, from the observations in Fig. 8, it is clear that this is no longer the case at lower BES-I energies. The particles and antiparticles are observed to separately follow the n_Q scaling in v_2 [82, 83]. (ii) At 7.7 and 11.5 GeV, the v_2 of the ϕ meson hints at being lower than that of the other hadrons (but much increased statistics are needed). The smaller v_2 values of the ϕ meson, which has a smaller hadronic interaction cross section, may indicate that hadronic interactions become more important than partonic effects for the systems formed at collision energies below 19.6 GeV [94, 95]. This aspect is discussed in further detail below. In addition, as suggested in Fig. 9, the baryon-meson splitting at intermediate p_T is reduced at the lower collision energies, which is consistent with the findings that hadronic interactions at these energies dominate in the systems formed.

The study of the v_2 of particles with a very small hadronic cross section may elucidate the partonic dynamics and collectivity in heavy-ion collisions. The ϕ meson, which is a bound state of the s and $\bar{s}$ quarks, has a small interaction cross-section with other hadrons, and freezes-out early [94, 95]. Due to this small hadronic interaction cross-section of the ϕ meson, its v_2 is almost unaffected by later-stage hadronic interactions, and will have a negligibly small value if ϕ mesons are not produced via s and $\bar{s}$ quark coalescence in the partonic phase [96].

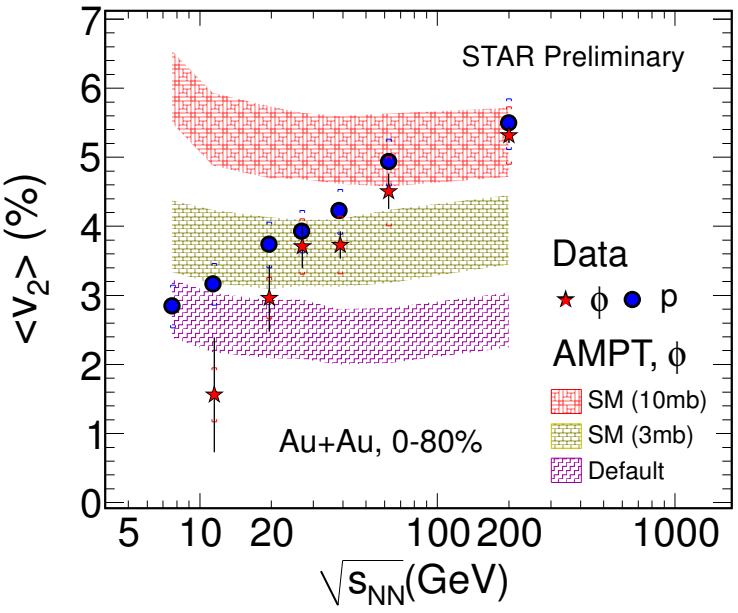

Figure 11. The p_T-integrated ϕ-meson and proton v_2 for Au+Au minimum-bias (0–80%) collisions at mid-rapidity ($|y| < 1.0$) at RHIC s a function of $\sqrt{s_{NN}}$. The ϕ meson v_2 values are compared to the corresponding AMPT model calculations at the same beam energies. Systematic errors on experimental data are shown by the cap symbol.

Figure 11 shows the p_T-integrated ϕ meson v_2 for Au+Au collisions as a function of $\sqrt{s_{NN}}$. The v_2 values increase with $\sqrt{s_{NN}}$. A comparison with the corresponding v_2 values for protons shows that the v_2 of ϕ mesons is consistent with that of the protons for $\sqrt{s_{NN}} > 19.6$ GeV. At center-of-mass energies below 19.6 GeV, the average v_2 of ϕ mesons seems to deviate from that of protons, as seen in Fig. 11.

The v_2 of ϕ mesons is compared to corresponding AMPT model calculations [97, 98] in Fig. 11. The $\langle v_2 \rangle$ values from the model remain constant for all the studied energies for a given parton-parton interaction cross-section, because it arises from the interactions between minijet partons. The $\langle v_2 \rangle$ of ϕ mesons for $\sqrt{s_{NN}} > 19.6$ GeV is consistent with the AMPT model with string melting enabled (AMPT-SM). The AMPT-SM model with a 10 mb parton-parton cross-section fits the data at $\sqrt{s_{NN}} = 62.4$ and 200 GeV, whereas a reduced value of the parton-parton cross-section of 3 mb is needed to describe the data at $\sqrt{s_{NN}} = 27$ and 39 GeV. The ϕ $\langle v_2 \rangle$ data at $\sqrt{s_{NN}} = 11.5$ GeV are consistent with the default framework of the AMPT model without needing partonic interactions.

The comparison with the AMPT model sheds some light on the collision dynamics. It suggests that below $\sqrt{s_{NN}} = 11.5$ GeV, the hadronic interactions may play a significant role, whereas above 19.6 GeV, there may be an increase in the contribution from partonic interactions.

2.4.2. Nuclear Modification Factor: One of the most exciting results at RHIC was the discovery of suppression in the production of high transverse momentum (p_T) mesons in

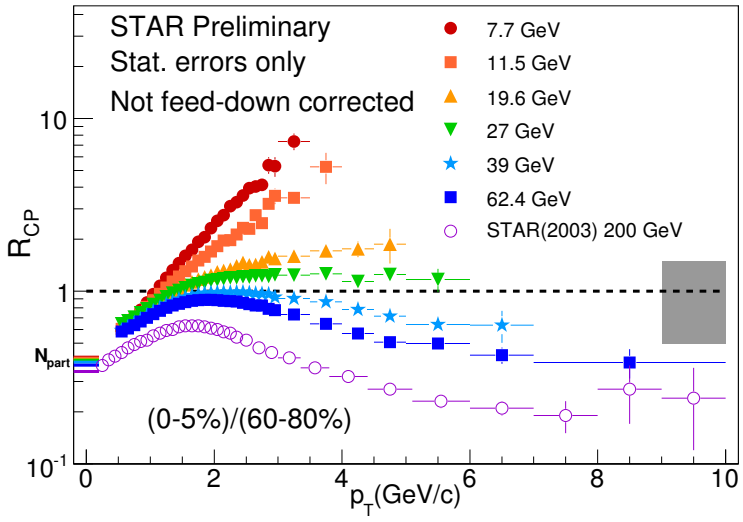

Figure 12. Nuclear modification factor versus transverse momentum for inclusive charged hadrons from Au+Au collisions at various $\sqrt{s_{NN}}$ at RHIC. The yield ratios for charged hadrons are taken for 0-5% to 60-80% collision centrality.

nucleus-nucleus collisions compared to appropriately scaled p+p collisions [73, 71, 99, 100]. This has been interpreted in terms of energy loss of partons in the QGP. This phenomenon is called jet quenching in dense partonic matter [101]. The energy loss by energetic partons in the dense medium formed in high-energy heavy-ion collisions is predicted to be proportional to both the initial gluon density [102, 103] and the lifetime of the dense matter [104]. High-p_T suppression results are usually presented in terms of a nuclear modification factor (R_{CP}), defined as

$$R_{CP} = \frac{\langle N_{\rm bin}^{\rm peri}\rangle\, d^3N_{AA}^{\rm cen}/d\eta\, d^2p_T}{\langle N_{\rm bin}^{\rm cen}\rangle\, d^3N_{AA}^{\rm peri}/d\eta\, d^2p_T}, \tag{2}$$

where the $N^{\rm cen}$ and $N^{\rm peri}$ correspond to particle yields in central and peripheral collisions, respectively. The $N_{\rm bin}^{\rm cen}$ and $N_{\rm bin}^{\rm peri}$ are the number of binary collisions for central and peripheral collisions, respectively, commonly estimated from a Glauber model [105].

Figure 12 shows the nuclear modification factor for inclusive charged hadrons from Au+Au collisions at each BES-I energy. The results at high p_T (> 2 GeV/c) show a smooth transition from strong enhancement at low beam energies to strong suppression at high beam energies. While it is clearly established that the suppression is related to the opacity of a deconfined medium of quarks and gluons, the source of enhancement could have multiple physics interpretations mostly related to dominance of hadronic interactions, like the Cronin effect, cold matter effects, or strong radial flow. Lack of baseline measurements from p+p and p+A collisions makes the quantitative interpretation of the measurements at lower beam energies difficult. Hence we need to resort to comparisons with various model-based calculations. On the other hand, it should be noted that PHENIX used p+p data sets at 39 and 62.4 GeV to create R_{AA} measurements. These agree qualitatively with the STAR results

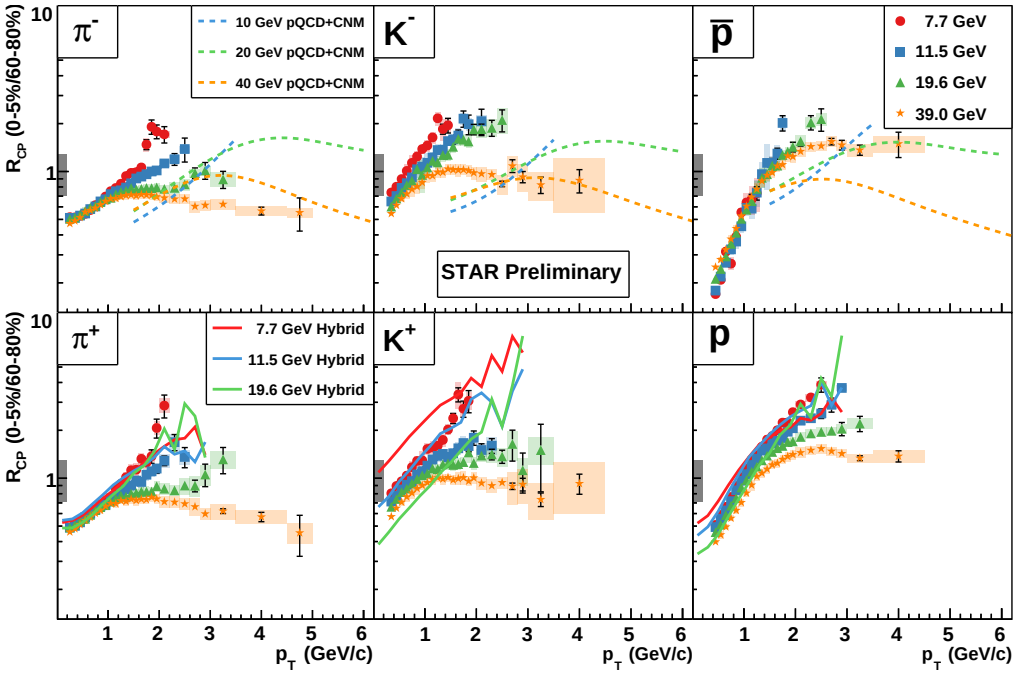

Figure 13. STAR data on the nuclear modification factor R_{CP} for π, K and p in Au+Au collisions. The central bin is 0-5% and the peripheral bin is 60-70%. In the upper three panels, pQCD calculations with next-to-leading order accuracy for 10, 20, and 40 GeV are compared to the BES-I data for negatively charged particles. In the lower three panels, Hybrid UrQMD+hydrodynamics calculations [52, 115, 116, 117] for 7.7, 11.5, and 19.6 GeV are compared to the BES-I data for positively charged particles.

shown in Fig. 12 [106].

Attempts to compare data to AMPT [97, 98] and HIJING [107] were made and both models failed to reproduce the experimental results. Calculations within the framework of perturbative QCD (pQCD) which focused predominantly, with varying degrees of sophistication, on the implementations of the energy loss of the leading parton or particle in the medium via radiative and collisional processes [108, 109] have explained the high-energy RHIC data to a large extent.

Studying the R_{CP} of identified particles may allow one to separate different effects, although this does limit the p_{T} reach as seen in Fig. 13. Advanced pQCD calculations [110], which include cold nuclear matter effects, for R_{CP} of identified hadrons [111, 112] in Au+Au collisions for $\sqrt{s_{NN}}$ = 10, 20 and 40 GeV are shown in the upper row of panels of the figure. The model calculations are compared to the corresponding STAR measurements at $\sqrt{s_{NN}}$ = 11.5, 19.6, and 39 GeV. The trend observed in the data is predicted correctly by the model, while the locations where the model predictions cross unity occur at p_T values that are about 1 GeV/c higher than experimentally observed.

The model formalism is based on the QCD factorization approach, augmented by cold nuclear matter and QGP effects. It incorporates the Cronin effect through the multiple

elastic scattering of partons in large nuclei, dynamical shadowing through coherent power corrections, and cold nuclear matter energy loss [111, 112]. For the kinematics at hand, the Cronin effect is the most important, and its competition with the QGP energy loss determines the predicted transition from enhancement to suppression for different $\sqrt{s_{NN}}$. The magnitude of nuclear effects is also determined by the steepness of the partonic spectra. Final state energy loss in the QGP is evaluated taking the soft gluon emission limit of full medium-induced splitting kernels [113, 114].

Even though the predictions at all center of mass energies include both the Cronin effect and the energy loss, the net result is an enhancement of R_{CP} at the lowest $\sqrt{s_{NN}}$ = 10 GeV and suppression at high p_T at the highest center of mass energy. The data enhancement over the model predictions at $\sqrt{s_{NN}}$ = 10 GeV could be an indication of the expected change in the medium degrees of freedom from gluon dominated at higest RHIC energies (larger energy losses in the medium compared to quarks and anti-quarks) to quark-antiquark dominated at the lower energies of 7.7 and 11.5 GeV. The difference may allow one to estimate the quark-to-gluon ratio at a particular energy. This is also consistent with the picture of hadronic interactions dominating the system formed in heavy-ion collisions at $\sqrt{s_{NN}}$ = 11.5 and 7.7 GeV. From the comparison with pQCD based calculations, it seems that the enhancement in R_{CP} observed is due to cold nuclear matter effects.

We now proceed to compare the data to a hybrid model [52, 115, 116, 117] where dynamics are dominated by bulk physics and not by jets. This hybrid model is based on the UrQMD transport approach with an intermediate hydrodynamical evolution for the hot and dense stage of the collision. The EOS used in the hydrodynamic part has a crossover for all μ_B [118]. Event-by-event fluctuations are directly taken into account via the non-equilibrium initial conditions generated by the initial collisions and string fragmentations in the microscopic UrQMD model. After a (3+1)-dimensional ideal hydrodynamic evolution, the hydrodynamical fields are mapped to hadrons via the Cooper-Frye equation and the subsequent hadronic cascade calculations proceed within the UrQMD framework; this incorporates the important final-state effects for a realistic freeze-out.

The lower panels of Fig. 13 compare R_{CP} for charged particles from the Hybrid model with STAR inclusive charged hadrons at $\sqrt{s_{NN}}$ = 7.7, 11.5 and 19.6 GeV. The p_T dependence of R_{CP} at small p_T at these lower beam energies is fairly well captured by the model. The model has stronger radial flow in central collisions compared to peripheral collisions, and this causes the enhancement in R_{CP} for the low energies. This implies that the data at these energies, and in the $p_{\rm T}$ range reached in BES-I, can be explained purely from a bulk physics perspective, and there is no need for invoking jet physics. With increasing beam energy and $p_{\rm T}$, jets will become more important, and one then observes the jet quenching effect.

The BES Phase-II program at RHIC, with significantly larger statistics, will allow STAR to reach high enough $p_{\rm T}$ to conclusively study the hard regime even at $\sqrt{s_{NN}}$ = 11.5 GeV. STAR will study the precise shape of R_{CP} and the position of the crossings at the various energies. This will help to constrain calculations and lead to an understanding of the contributions and interplay between various physical processes (including hard and soft) involved in relativistic heavy-ion collisions.

2.4.3. Dynamical Charge Correlations: In QCD, chiral symmetry breaking and the origin of hadron masses are related to the existence of topologically nontrivial classical gluonic fields, instantons, and sphalerons, which describe the transitions between the vacuum states with different Chern-Simons numbers. Quark interactions with such fields change the quark chirality and are $\mathcal{P}$ and $\mathcal{CP}$ odd. Such a theoretical proposition had never been observed directly in experiments. It was soon realized that an experimental search for local strong parity violation (LPV) is possible in heavy-ion collisions [119, 120]. For such a phenomenon where the massless quarks can change their chirality due to interactions with gluon fields, there could be separation of positive charges from negative charges along the direction of the angular momentum of the collision, as a result of the large magnetic fields ($\sim 10^{15}$ T) produced in non-central collisions. This phenomenon is also called the chiral magnetic effect (CME) [120, 121, 122]. The CME needs the system to be deconfined, as that allows for the possibility of quarks traveling over distances greater than nucleonic scales, and also requires chiral symmetry restoration, since a chiral condensate will tend to erase any asymmetry between the number of right- and left-handed fermions. Observation of CME at top RHIC energy [123, 124] and its absence at lower beam energy would be considered evidence of a turn-off of one of the QGP signatures.

A three-point correlator, $\gamma \equiv \langle \cos(\phi_\alpha + \phi_\beta - 2\Psi_{\rm RP}) \rangle$, sensitive to the CME was proposed in Ref. [125], where ϕ is the azimuthal angle, the subscripts α and β denote the particle charge (positive or negative), and $\Psi_{\rm RP}$ is the angle of the reaction plane of a given event. The observable γ represents the difference between azimuthal correlations projected onto the direction of the angular momentum vector and correlations projected onto the collision event plane. The STAR measurements [74, 75] of this correlator for Au+Au collisions at 200 GeV shown in Fig. 14(b) demonstrate the "right" ordering of the opposite charge ($\gamma_{\rm OS}$) and the same charge ($\gamma_{\rm SS}$) correlations, supporting the picture of the CME. This is consistent with the formation of deconfined and chirally-symmetric restored matter in high energy heavy-ion collisions. The signal is robust to various ways of determination of the reaction plane [123], and persists when the collision system changes to Cu+Cu [74, 75] or Pb+Pb [124].

An ambiguity in the interpretation of experimental results comes from possible background correlations not related to CME [75]. The background sources, if coupled with collective flow, will also contribute to γ. Ref. [126] suggests that $(\gamma_{\rm OS} - \gamma_{\rm SS})$ measured by STAR can be explained within a blast wave model that includes charge conservation, with radial and elliptic flow.

Figure 14 presents $\gamma_{\rm OS}$ and $\gamma_{\rm SS}$ correlators for Au+Au collisions at $\sqrt{s_{NN}} = 7.7 - 200$ GeV as a function of centrality. In addition, the ALICE measurements [124] for 2.76 TeV Pb+Pb collisions are shown. The ordering of $\gamma_{\rm OS}$ and $\gamma_{\rm SS}$ is present as in collisions at the higher energies [74, 75, 124]. This is consistent with extra charge-separation fluctuations perpendicular to the reaction plane due to the CME. At lower beam energies, both $\gamma_{\rm OS}$ and $\gamma_{\rm SS}$ tend to rise for peripheral collisions. This feature seems to be charge independent, and is explained by momentum conservation and elliptic flow [123]. For peripheral collisions, the multiplicity (N) is small, and momentum conservation dominates. For more central collisions, where the multiplicity is large enough, this type of $\mathcal{P}$-even background can be estimated by

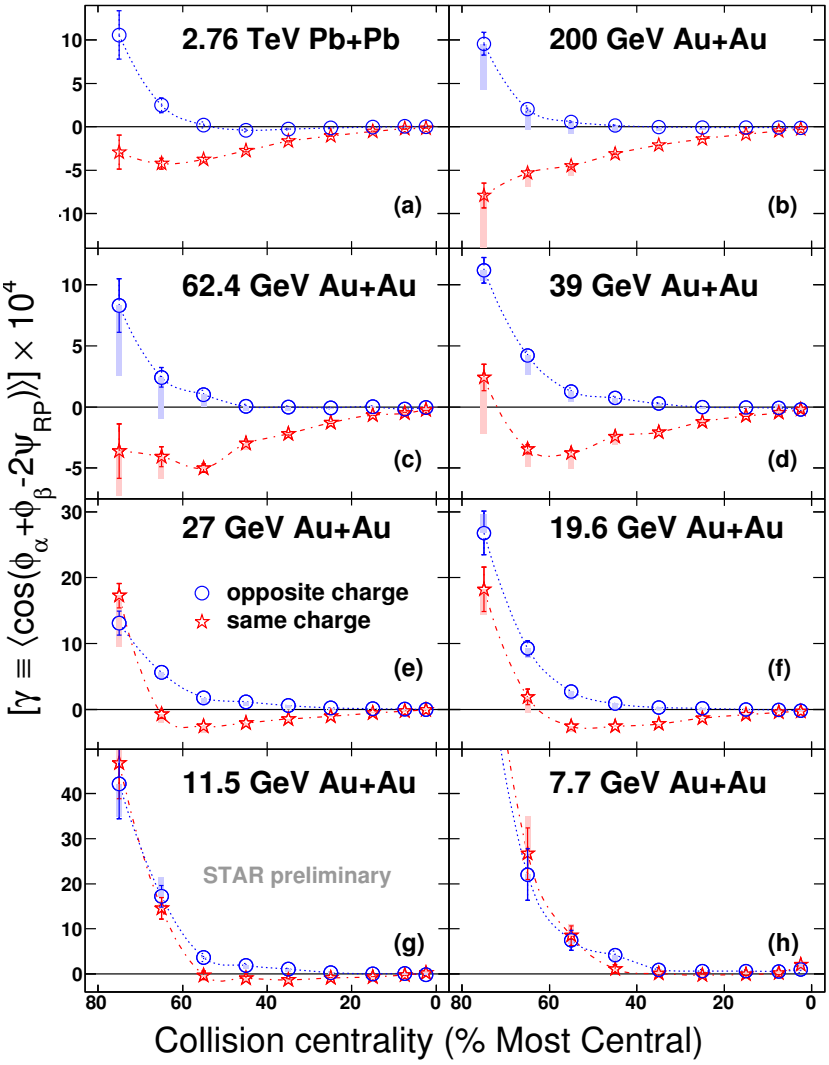

Figure 14. The three-point correlator (γ) as a function of centrality for Au+Au collisions at $\sqrt{s_{NN}}$ = 7.7-200 GeV. Also shown are the corresponding results for Pb+Pb collisions at $\sqrt{s_{NN}}$ = 2.76 TeV from ALICE at the LHC [124]. Note that the vertical scales are different for the different rows. The plotted systematic errors (shaded rectangles) reflect the extra conditions of $\Delta p_T > 0.15$ GeV/c and $\Delta\eta > 0.15$ to suppress HBT + Coulomb effects.

$-v_2/N$ [123, 127].

In order to separate the signal associated with the CME from that due to the background contributions, we can express the experimental observables in the following forms, where the unknown parameter κ, as argued in Ref. [128], is of the order of unity.

$$\gamma \equiv \langle\cos(\phi_1+\phi_2-2\Psi_{\rm RP})\rangle = \kappa v_2 F - H \tag{3}$$

$$\delta \equiv \langle\cos(\phi_1-\phi_2)\rangle = F + H\,, \tag{4}$$

where H and F are the CME and background contributions, respectively. Figure 15 shows $H_{\rm SS} - H_{\rm OS}$ as a function of beam energy for three centrality bins in Au+Au collisions. The default values (dotted curves) are from $H^{\kappa=1}$, and the solid (dash-dot) curves are obtained

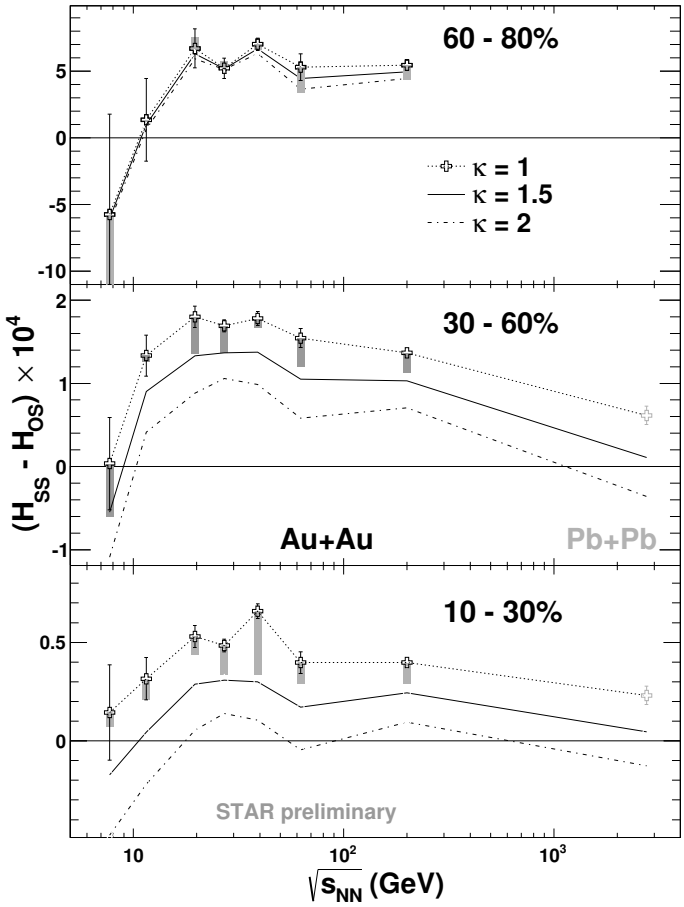

Figure 15. $(H_{\rm SS} - H_{\rm OS})$ is shown as a function of beam energy for three centrality bins. The default values (dotted curves) are from $H^{\kappa=1}$, and the solid (dash-dot) curves are obtained with $\kappa = 1.5$ ($\kappa = 2$). For comparison, the results for Pb+Pb collisions at 2.76 TeV are also shown [124]. The plotted systematic errors have the same meaning as in Fig. 14.

with $\kappa = 1.5$ ($\kappa = 2$), where κ is a parameter that could account for finite detector acceptance and for theoretical uncertainties. For comparison, results for $10-60\%$ Pb+Pb collisions at 2.76 TeV are also shown [124]. In the case of $\kappa = 1$, $(H_{\rm SS} - H_{\rm OS})$ demonstrates a weak energy dependence above 19.6 GeV, and trends toward zero at the lowest beam energy, although the statistical errors are large for 7.7 GeV. This may be explained by the probable dominance of hadronic interactions over partonic ones at the lowest energies. With increased κ, $(H_{\rm SS} - H_{\rm OS})$ decreases for all beam energies and may even totally disappear in some cases (e.g. with $\kappa \sim 2$ in $10-30\%$ collisions). If better theoretical estimates of κ are available in the future, a more conclusive result could be extracted from Fig. 15 with interpolation or extrapolation of the data. The energy for which $(H_{\rm SS} - H_{\rm OS})$ = 0 will be determined quantitatively with higher statistics in BES Phase-II.

2.4.4. Chiral Transition and Dileptons: Electromagnetic observables, such as photons and dileptons, are ideal probes and are emitted throughout the evolution of a heavy-ion collision,

thus carrying information about all the stages of the reaction [129, 130]. As leptons are inert to the strong force, there will be negligible interactions in the medium, hence they are considered to be ideal penetrating probes. Apart from Dalitz decays, prominent sources of dileptons in the low invariant-mass range (LMR: $M_{ee} < 1.1$ GeV/c^2) are direct leptonic decays of the $\rho(770)$, $\omega(782)$, and $\phi(1020)$ vector mesons. The ρ meson is of special interest given that in thermal equilibrium, its contribution to the low mass range is expected to dominate through its strong coupling to the $\pi\pi$ channel. Moreover, its short lifetime $\tau = 1.3$ fm/c makes its spectral shape especially sensitive to in-medium modifications, a proposed signature of chiral symmetry restoration [131].

At SPS energies, the apparent low-mass dilepton enhancement observed in both the CERES dielectron [132] and NA60 dimuon data [133] can be explained in terms of in-medium modifications of the spectral shape of the ρ meson. The dimuon measurements by NA60 are found to favor significant broadening of the ρ meson line shape over a mass-dropping scenario [134, 135, 136, 137]. At top RHIC energies ($\sqrt{s_{NN}}$ = 200 GeV), both the PHENIX [138] and STAR [139] collaborations have observed a significant enhancement in the low-mass dielectron measurements. Models that have been able to describe the measurements at SPS energies can describe the enhancements seen at RHIC, with the exception of results from PHENIX for the most central collisions.

Dilepton measurements in the intermediate invariant mass range (IMR), typically defined to be between the masses of the ϕ and J/ψ mesons, are sensitive to thermal radiation from the QGP [4]. However, contributions from semi-leptonic decays of open heavy-flavor hadrons are significant for the higher RHIC beam energies. In the BES-I program, such direct measurements could not be performed. With STAR's recently improved muon detection capabilities, however, direct measurements of e-μ correlations should in the future help establish the open heavy-flavor contributions.

The BES-I program has put STAR in a unique position to systematically measure dielectron spectra in the low and intermediate mass ranges from SPS center-of-mass energies to the top RHIC energies, $\sqrt{s_{\rm NN}} = 200$ GeV. Figure 16 shows the dielectron invariant mass distributions extending out to the J/ψ mass for minimum-bias (0 - 80%) Au+Au collisions at beam energies from $\sqrt{s_{\rm NN}}$ =19.6 up to 200 GeV. Dielectron measurements are statistically challenging due to very low signal-to-background ratios. Compared to a total minimum-bias sample of about 770M events at $\sqrt{s_{\rm NN}} = 200$ GeV (Fig.16 only involves 260M events) BES-I only reached 36M, 130M, and 67M events, for $\sqrt{s_{\rm NN}}$ =19.6, 39, and 62.4 GeV, respectively (see Table 1). Consequently, in the intermediate mass range, the statistical uncertainty for the lower beam energies is very large, and complicates a meaningful interpretation of the results.

In Fig.17, the efficiency-corrected invariant mass spectra are shown for minimum-bias Au+Au collisions at $\sqrt{s_{\rm NN}} = 19.6$, 39, 62.4, and 200 GeV. The hadron cocktail simulations include contributions from Dalitz decays and dielectron decays of the ω and ϕ vector mesons. Contributions from ρ mesons have been excluded from the cocktail, but are explicitly included in the model calculations in [140]. It has been noted that while the free emission rates of dileptons in the QGP and hadron gas phase are very different, the in-medium rates in both phases approach each other when extrapolated into the expected phase transition region [141].

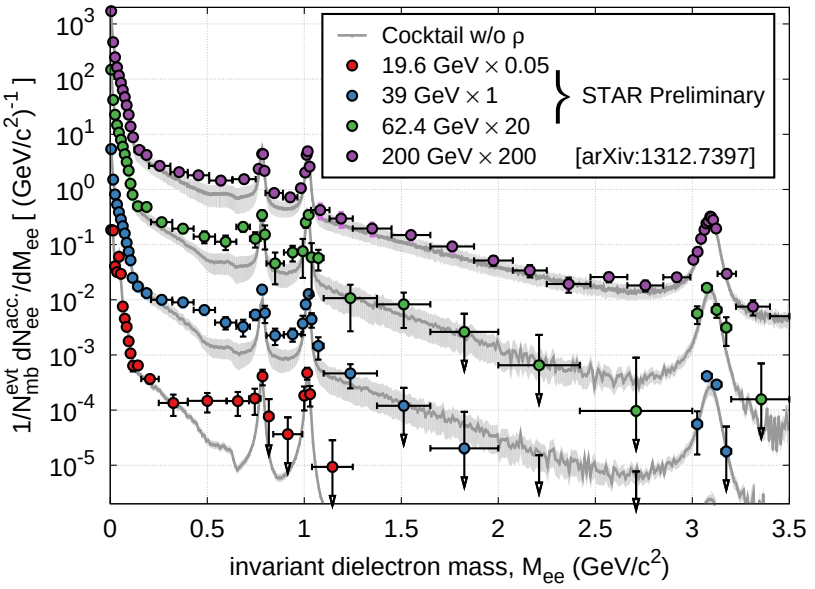

Figure 16. Background-subtracted dielectron invariant-mass distributions from Au+Au collisions at $\sqrt{s_{\rm NN}}$ = 19.6, 39, 62.4, and 200 GeV. The (colored) dotted lines show the hadron cocktails (excluding contributions from ρ mesons). The (color) shaded areas indicate systematic uncertainties.

It was also noted in Ref. [142] that the degeneracy of the top-down extrapolated pQCD and the bottom-up hadronic many-body calculations indirectly implies chiral symmetry restoration, since in pQCD, the vector and axial vector components are degenerate. When compared with the experimental results, the model calculations provide a robust description from top RHIC energies down to SPS energies. Furthermore, this observation agrees with the expectation that medium effects are driven by the strong coupling to baryons, and thus to the total baryon density, since the ρ mesons interact symmetrically with baryons and antibaryons [143].

At SPS beam energies, with substantial nuclear stopping, most baryons are participating nucleons. At RHIC top energies, on the other hand, the net-baryon density largely vanishes, while a significant baryon-antibaryon production is expected to compensate the total baryon density. The total baryon density at freeze-out as a function of $\sqrt{s_{\rm NN}}$, as shown in Fig. 18, does not change significantly with center-of-mass energies above 20 GeV. Accordingly, models that show good agreement at SPS and top RHIC energies should be able to describe the low-mass enhancement throughout the BES-I energy range.

STAR's systematic LMR dielectron measurements during BES-I allowed models to tie recent results at top RHIC energies to (top) SPS energies. The preliminary results illustrate how the measured excess develops as a function of the beam energy while the total baryon density remains approximately similar as can be seen in Fig. 18. Taking the measurements to beam energies below 19.6 GeV would provide further opportunity to compare to SPS measurements [132] at 40 *A* GeV fixed-target energies.

While the LMR measurements provide a way to study the chiral symmetry restoration,

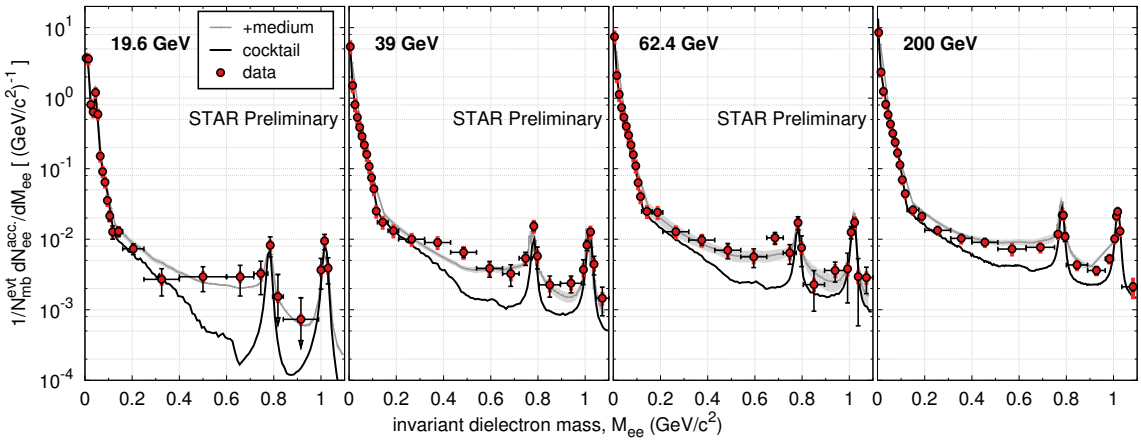

Figure 17. BES-I dielectron invariant mass distributions in the low invariant-mass range from Au+Au collisions at $\sqrt{s_{\rm NN}}$ = 19.6, 39, 62.4, and 200 GeV. The 39 and 62 GeV measured spectra have both been scaled to the cocktail π^0 yields. The black curves depict the hadronic cocktail and include all known hadronic sources with the exception of the ρ meson. The grey curves depict model calculations [140] which include contributions from both the hadron gas and QGP phases.

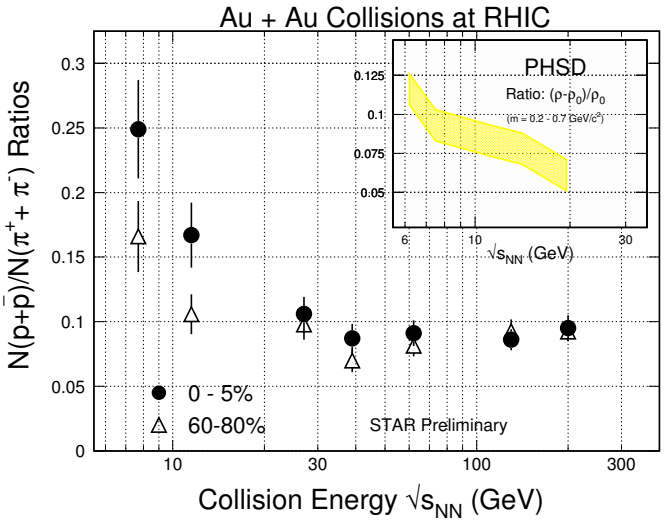

Figure 18. STAR measurements of $(\mathrm{p}+\bar{\mathrm{p}})/(\pi^+ + \pi^-)$ in Au+Au collisions as a function of the center-of-mass energy $\sqrt{s_{\rm NN}}$ are shown for the 0-5% (circles) and 60-80% (triangles) centralities. The shaded area in the in-set indicates PHSD model predictions for the in-medium ρ yield as determined in the invariant dielectron mass range of 0.2 to 0.7 GeV/c^2 in minimum-bias Au+Au collisions [144].

the duality of the dilepton rates around $T_{\rm c}$ will make it difficult to separate the relative contributions from the QGP or hadron gas phases. Instead, with its blue-shift-free invariant mass slope, the IMR is sensitive to changes of $T_{\rm c}$. Using the relation between the real photon and virtual photon production, measured via the associated dielectric production, one can study the properties of the QGP. In addition, for $p_{\rm T} > 6$ GeV/c, one can also study the photon

production in the primordial phase of the collision. The limited statistics collected during BES-I was too small for meaningful measurements in the intermediate mass range.

One of the most important objectives of the beam energy scan is the search for the critical point. A system close to the critical point will see an increase in its correlation lengths, and hence relaxation rates will exhibit critical slowing down. Because total dilepton yields are sensitive to the duration of emission, an *anomalous* increase in the lifetime of the fireball would be detectable through an increase in the dilepton yields [145]. It should be noted that in some models, the critical slowing down is completely governed by soft hydro modes and this complicates the relationship between the lifetime of the system and the dilepton yields. With an accuracy of ± 1 fm/c, NA60's lifetime measurements [146] at $\sqrt{s_{\rm NN}} = 17.3$ GeV did not provide any evidence of such anomalous increases in a notably smaller system of In+In collisions. However, in model calculations, most EM radiation occurs around $T_{\rm c}$, thus making the dilepton channel sensitive for lifetime changes that occur around this region. Consequently, a change in lifetime of 25% could result in a yield increase up to 40%.

3. Proposal for BES Phase-II

3.1. Overview

The proposal for BES Phase-II is driven by the precision requirements for the suite of physics measurements identified, based on the BES-I results, to be the most discriminating in the effort to better understand the phase diagram of QCD matter. Below, we list the key observables and describe the requirements and statistics needs for each. The following descriptions then form the basis for the event statistics estimates given in Table 2. These in turn allow for a determination of the optimal run strategy, which is detailed in Table 3.

- *R_{CP} of identified hadrons up to p_T = 5 GeV/c:* This will enable us to understand the underlying physics (soft versus hard) driving the shape of $R_{CP}(p_T)$ and quantitatively address the evolution of the phenomenon of jet-quenching to lower beam energies. Although the BES-I data show suggestive features, the spectra run out of statistics at p_T between 3 and 4 GeV/c. These spectra do not reach high enough p_T to extend into the purely hard-scattering regime. However, they do allow us to make detailed projections of how many events would be needed to reach a given p_T for a given beam energy. We propose to acquire about 400 tracks in the p_T range of 4-5 GeV/c for the 11.5, 14.5, and 19.6 GeV energies. At the lower energies of 7.7 and 9.1 GeV, there is simply not enough kinematic reach to get out to 4-5 GeV/c.
- *The centrality dependence of the slope of $v_1(y)$ around midrapidity:* Results from BES Phase-II will consolidate the findings of a non-monotonic variation in the slope of $v_1(y)$ for protons and net protons. It is proposed to study the centrality dependence of v_1 by taking high statistics data with the detector upgrades discussed below. The proposed statistics at each energy will allow us to measure the centrality dependence of the slope of v_1 in a step size of 5% in centrality for protons, antiprotons, and net protons, each with

comparable statistics as achieved in our BES-I analysis, which focused on only a single wide bin (10-40% centrality).

- *The v_2 of ϕ mesons and high p_T NCQ scaling for indentified particles:* This measurement will allow us to quantitatively address the suspected absence of partonic collectivity below $\sqrt{s_{NN}}$ = 19.6 GeV. High-statistics data with a new event plane detector (as discussed below) are required. It is necessary to make measurements up to p_T = 3 GeV/c with a statistical error of less than 10% on v_2. With the increased statistics, BES Phase-II will reach transverse momenta for the identified particle elliptic flow measurement beyond 2.5 GeV/c even at the lowest energies. This will allow us to test in NCQ scaling detail for many particle species, including multi-strange particles, in the relevant p_T range.
- *Three-particle correlators related to CME/LPV:* These measurements will allow us to corroborate the observation of the turn-off of CME/LPV-like effects at 7.7 GeV. In order to reduce the statistical error on the measured CME signal $H_{SS} - H_{OS}$ by a factor 3, we propose to increase the event statistics by factors of ten and four at 7.7 and 11.5 GeV, respectively. This requires $\sim$ 50M events for each beam energy.
- *Improved $\kappa\sigma^2$ for net-protons:* These proposed improvements will allow us to quantitatively establish the variation of net-proton $\kappa\sigma^2$ with beam energy. The current measurements have large statistical uncertainty at $\sqrt{s_{NN}}$ = 7.7 and 11.5 GeV, which precludes any conclusion of a non-monotonic or monotonic variation of the observable with beam energy. We will need to achieve a statistical error of less than 10% on $\kappa\sigma^2$ for each beam energy.
- *Two-particle correlations:* The interesting BES-I results on net-proton v_1 and $\kappa\sigma^2$ suggest that one should further explore the correlations among the protons. Azimuthally sensitive measurements for pairs of protons are envisioned. This will allow a measurement of the baryon coordinate-space anisotropy and the orientation of the participant ellipsoid with respect to the beam axis [147, 148, 149]. The expected tilt of the proton source can be directly related to the directed flow measurements for protons. The result will help elucidate the expansion and evolution of the system. In addition, we will perform the measurements of identical and non-identical particle correlation functions, between pions, kaons, and protons, because the systematic measurements will help us to extract the space-time-momentum correlation which is driven by the EOS of the system. The required statistics for the azimuthally-sensitive measurement for protons at different collision energies are listed in Table 2. The estimation was made based on the information from BES-I pion azimuthally-sensitive HBT data [150], proton-to-pion ratios, and the expected strength of the directed flow and its correlation to the tilt angle [151, 152, 153].
- *Dilepton production:* With low material budget and large acceptance, STAR has the unique opportunity to carry out a systematic study of dilepton production in high net-baryon density environments. Having established the capability to do such measurements at higher energies, we propose to extend the same to lower beam energies. The

Table 2. Event statistics (in millions) needed for Beam Energy Scan Phase-II for various observables.

Collision Energy (GeV)	7.7	9.1	11.5	14.5	19.6
μ_B (MeV) in 0-5% central collisions	420	370	315	260	205
Observables					
R_{CP} up to p_T = 5 GeV/c	–		160	125	92
Elliptic Flow (ϕ mesons)	100	150	200	200	400
Chiral Magnetic Effect	50	50	50	50	50
Directed Flow (protons)	50	75	100	100	200
Azimuthal HBT (protons)	35	40	50	65	80
Net-Proton Kurtosis	80	100	120	200	400
Dileptons	100	160	230	300	400
Required Number of Events	**100**	**160**	**230**	**300**	**400**

requirement in the LMR is to achieve a similar level of statistical uncertainty as is reached for STAR's $\sqrt{s_{\rm NN}}$ =200 GeV data sample. Based on the BES-I 19.6 GeV data sample of less than 40M events, this would imply about 400M minimum-bias events at that particular energy. As the signal-to-background ratio is expected to improve for the lower energies due to a significant reduction of the combinatorial background and the c-$\bar{c}$ continuum, the required event samples are reduced by factors of up to ~ 4 for the lowest energies. The improvement needed in the IMR is estimated based on the statistical uncertainties of the dielectron mass slope from the same BES-I data set at $\sqrt{s_{\rm NN}}$ = 19.6 GeV. A factor of 10 more (minimum-bias) events would bring that uncertainty to about 10%. Note that this is comparable to the requested improvement in statistics for the LMR measurements.

Table 2 summarizes the BES Phase-II proposal, based on the assumption that there will be 22 cryo-weeks of RHIC running in each of the years 2018 and 2019. The proposed number of weeks of RHIC running at 7.7 GeV has been estimated by considering the corresponding average event rate in the final week of BES-I operations, BES-I luminosity, an electron cooling luminosity improvement factor mid-way between the optimistic and pessimistic estimates, and the number of events required for the physics program as per Table 2. The proposed number of weeks for beam energies of 11.5 and 19.6 GeV are obtained using the average numbers for event rate and luminosity over the entire collider running period, and the event statistics as desired in BES Phase-II (Table 2). There is an additional uncertainty on the rate estimates for the 19.6 GeV system, and that arises because without an improvement to the trigger, the raw data rate will exceed the limits of the STAR DAQ system. The situation should be significantly improved with the help of the cleaner beam after electron cooling, and with the help of the Event Plane Detector (EPD) upgrade described below. The proposal for the number of weeks of RHIC running at 9.1 and 14.5 GeV are estimated by interpolating the required numbers between the adjacent energy points.

The sum of the requests over all beam energies is 35 weeks. Adding one week of setup for each energy, and allowing two weeks of cool-down (warm-up) at the start (end) of each

Table 3. Beam Energy Scan Phase-II proposal for 22 weeks of RHIC running in each of the years 2018 and 2019.

Collision Energy (GeV)	7.7	9.1	11.5	14.5	19.6
μ_B (MeV) in 0-5% Central Collisions	420	370	315	260	205
BES-I (Million Events)	4	–	12	20	36
Event Rate (Million Events/Day)	0.25	0.6	1.7	2.4	4.5
BES-I Int. Luminosity (1×10^{25}/cm^2 s)	0.13	0.5	1.5	2.1	4.0
e-Cooling Luminosity Improvement Factor	4	4	4	8	15(4)
BES Phase-II (Million Events)	100	160	230	300	400
Required Beam Time (Weeks)	14	9.5	5.0	2.5	4.0+

year, brings the grand total to 44 weeks. The approach outlined in Table 3 is the optimal strategy based on the information available at this time. There will also be lessons learned in the first year of the BES Phase-II program that may cause us to re-think the priorities for the second year. A possible scenario is to spend the first year of the program taking data sets at each of the five proposed energies, and then determine if it is the best use of accelerator time to complete the beam-time-intensive 7.7 and 9.1 GeV runs, or whether there might be key physics that could be accessed with more time at a higher energy, or via a pivot to new intervening energies. For example, a meaningful measurement of J/ψ could be made at 19.6 GeV with a data sample of approximately 1 billion events. Optimistic estimates of the performance for the collider and for STAR could make this target achievable. However, this document has taken a conservative approach to count-rate estimates. These estimates can be refined considerably following the first year of running with electron cooling.

3.2. The Fixed-Target Program

Several observables show intriguing threshold behavior at roughly $\sqrt{s_{NN}}$ = 7.7 GeV, see Fig. 7 and Ref. [13]. These observations have been used to suggest that this energy corresponds to the onset of deconfinement [13, 154]. In order to test this conjecture, the RHIC BES Phase-II program could benefit from studying energies below 7.7 GeV. These lowest energies have proven to be challenging for the collider. However, it has been demonstrated that with the addition of a gold target placed inside the beampipe, energies of $\sqrt{s_{NN}}$ = 3.0, 3.2, 3.5, 4.0, and 4.5 GeV could be studied. These energies correspond to collisions between gold projectiles tuned for collisions at 7.7, 9.1, 11.5, 14.5, and 19.6 GeV respectively and the gold fixed-target. By tuning the collider for 62.4 GeV collisions, it will be possible to take a fixed-target dataset at $\sqrt{s_{NN}}$ = 7.7 GeV, thus providing a cross-check between the fixed-target and the collider programs. The primary physics goals of this part of the program will focus on observables which are sensitive to a softening of the equation of state, as it is expected that the first entry into the mixed-phase will occur at energies below the onset of deconfinement [155, 156, 157]. In addition, the fixed-target results will serve as important controls for the critical point and QGP studies of the BES Phase-II collider program.

3.3. The Importance of p+p and p+A Systems

In order to fully understand heavy-ion collisions at a given collision energy, and particularly to understand the partonic stage, it is important to measure nucleon-nucleon collisions and cold matter matter effects at that energy. Generally, p+p and p+A collisions supply the proper reference to allow the effects of the initial states to be identified, measured, and separated from those which are due to the partonic medium, which is assumed to be formed only in heavy-ion collisions. Therefore, the ideal BES Phase-II would have a companion p+p and p+A scan program which would cover the same collision energies. Collisions of p+p are also essential for dielectron measurements, to prove cocktail consistency as a baseline for Au+Au. These measurements are so far missing in the BES region and would significantly reduce cocktail uncertainties and help in the extrapolation of yields from SPS to top RHIC energies. However, the BES Phase-II is focusing on an energy region below RHIC injection energy (19.6 GeV), and the higher charge-to-mass ratio of the proton with respect to gold nuclei allows only for p+p and p+A collisions at energies of 19.6 GeV and above. Studying p+p and p+A collisions at 19.6 GeV indeed might prove to be extremely important. However, as our current view is that the highest-priority energies lie at the lower end of the search range, we will resort to using peripheral collisions as our proxy for the p+p reference data. It should be noted that peripheral collisions are not an alternative option for the dilepton measurements.

3.4. Collider Performance

As discussed above, the major thrust of the BES Phase-II program is to make high statistics measurements of the observables presented in this document for Au+Au collisions at $\sqrt{s_{NN}} <$ 20 GeV. This requires the operation of RHIC with luminosities significantly increased over those which were achieved during BES-I. This can be accomplished by constructing an electron cooling system to reduce the transverse beam emittance and by developing the ability to stretch the bunches longitudinally to reduce the intra-beam Coulomb scattering.

The original design of RHIC optimized the luminosity at $\sqrt{s_{NN}}$ = 200 GeV. At lower energies, the beam is not as well-focused and the collision rate is low. In order to provide adequate intensity for BES Phase-II, the RHIC Collider Accelerator Division has been undertaking an upgrade with electron cooling (Fig. 19). According to simulations, with the proposed electron superconducting RF gun, the luminosity will increase by a factor of 2-5 at $\sqrt{s_{NN}}$ = 7.7 GeV and by a factor of 8-20 at $\sqrt{s_{NN}}$= 20 GeV. Additional luminosity increases will be made possible by stretching the beam bunches beyond the usual 6 ns length.

All of these advances makes it very realistic to achieve the event statistics required for the key measurements listed in Table 2.

3.5. Detector Upgrades

Motivated by BES Phase-II physics goals, the following aspects of STAR measurements would greatly benefit from improvements and upgrades of the existing STAR detector system.

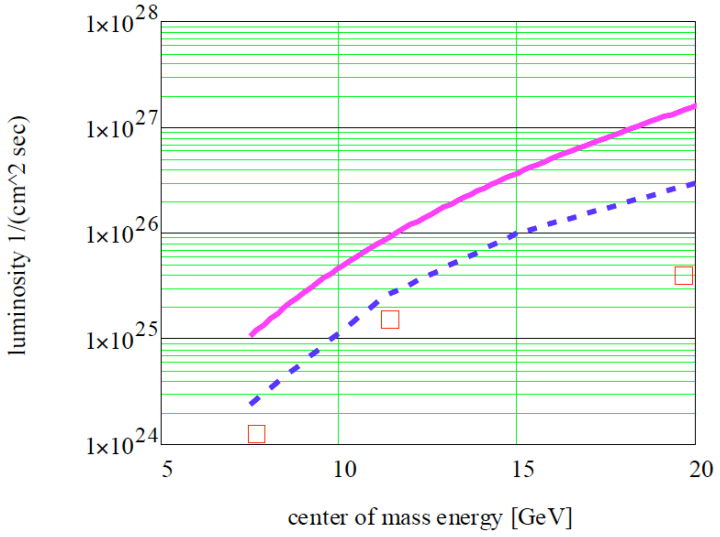

Figure 19. Projection of averaged store luminosity within ± 1 m vertex for Au ions in RHIC. The lines represent the optimistic (red) and pessimistic (blue) estimates for the luminosity which will be achieved with electron cooling. The open squares are the luminosities reached in BES-I.

- *Better acceptance for the STAR TPC in rapidity and p_T:* (i) This will enable the study of rapidity dependence of freeze-out dynamics. For a given beam energy, going towards higher rapidity offers the possibility of extending the μ_B range, thereby scanning a larger part of the phase diagram. (ii) It will extend measurements of v_1 beyond the information contained in the slope of $v_1(y)$ close to midrapdity. A broadened rapidity acceptance will expand our understanding of the role of baryon transport on the v_1 measurements. (iii) It will permit study of the rapidity dependence of higher moments of net-proton/net-charge distributions, to understand the role of charge/baryon number conservation, and to provide an experimental approach to determine the optimum phase space required to capture critical fluctuations and reduce the effect of centrality resolution on the higher moments [43]. (iv) It will improve the low p_T acceptance, which will better constrain the physics of freeze-out dynamics, by reducing the systematic uncertainties associated with extracting the yields of various particles. (v) It will improve the strange and multi-strange hadron reconstruction efficiency, which will strengthen quantitative conclusions about partonic collectivity.
- *Centrality determination:* Currently, STAR uses the charged particle multiplicity measured in the TPC to determine the collision centrality. Fluctuation and correlation measurements are particularly sensitive to possible correlations between the charged tracks used for physics analysis and those used for centrality determination. This is best avoided, and will be achieved if collision centrality is determined from a separate detector in a different pseudorapidity region from the TPC.
- *Event-plane determination:* Measurements of elliptic flow in BES-I used the TPC for the event plane determination. Non-flow effects have been reduced by keeping an η gap

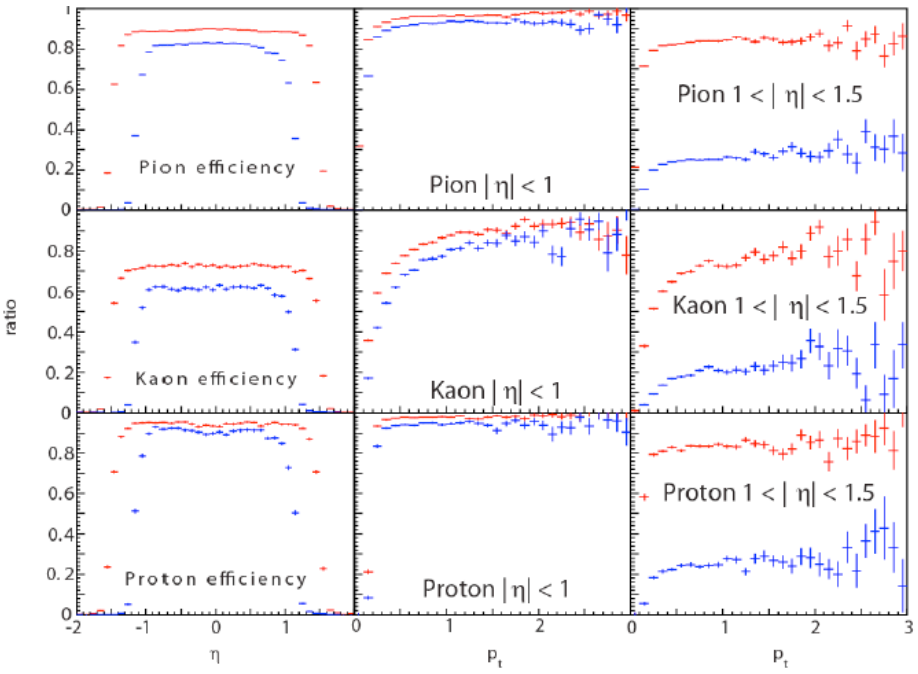

Figure 20. Pseudorapidity and transverse momentum dependence of the detection efficiencies for pions (top panel), kaons (middle panel), and protons (bottom panel). Blue and red points are the results for TPC and iTPC, respectively [158].

(currently ~ 0.1– 0.2) between the particles used for the correlation measurement and the event plane measurement. A dedicated event-plane detector centered at a pseudorapidity of 3 units would result in an η gap of about 2 units of pseudorapidity and thus would limit non-flow effects to a minimum. Directed flow measurements in BES-I used the BBC detectors, which have poor event-plane resolution. A dedicated event-plane detector would improve physics performance and facilitate physics interpretation in such analyses also.

- *Trigger performance:* The transverse beam size at the lowest RHIC energies was significantly greater than at $\sqrt{s_{NN}} = 200$ GeV, causing collisions of ions in the beam halo with either the beam pipe or support-structure materials. At $\sqrt{s_{NN}} = 7.7$ GeV, 80–98% of the triggered reactions came from such beam on beam-pipe collisions. The situation will improve with the installation of an electron gun. A total increase in luminosity of about a factor 10 is expected, which will result in a trigger rate of several kHz at the highest BES energy. To exploit this, it is essential to trigger on all good Au+Au collisions with a reconstructible vertex.

iTPC: It is proposed [158] to upgrade the inner sectors of the STAR TPC to increase the segmentation on the inner pad plane and to renew the inner-sector wires, which are showing signs of aging. The upgrade will provide better momentum resolution, better dE/dx resolution, improved acceptance at high rapidity to $|\eta| < 1.7$ compared to the current TPC configuration of $|\eta| < 1.0$, and higher track reconstruction efficiency. Although iTPC will

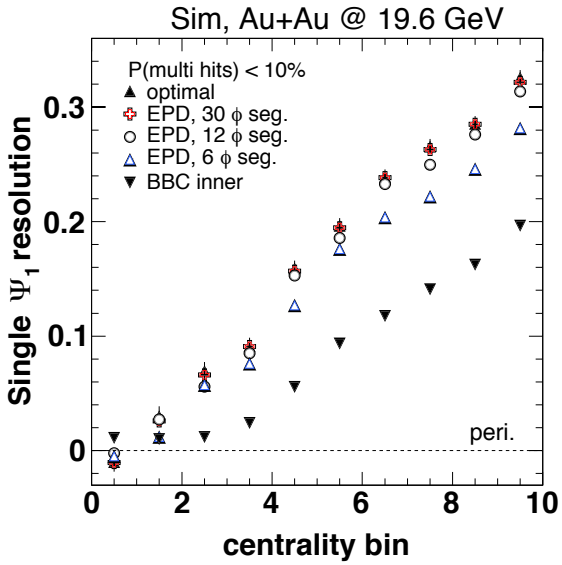

Figure 21. First-harmonic event-plane resolution as a function of collision centrality for different detector segmentations [159].

allow significantly improved tracking and coverage out to $|\eta| < 1.7$, the longitudinal boost for higher rapidity particles shifts the low p_{T} particles into a momentum range where it becomes increasingly challenging to employ PID through relative ionization in the TPC. The PID capabilites will be supplemented with the inclusion of one prototype sector of the End-Cap Time-of-Flight (eTOF) [160]. Although the eTOF prototype will only have a narrow azimuthal acceptance, this will enable key inclusive measurements. The enhanced performance made possible by the iTPC will not only benefit the BES Phase-II physics program but will also be crucial for STAR's future program with p+p/p+A and ep/eA collisions at forward higher-rapidity regions. Figure 20 shows the improved acceptance in p_{T} and y for reconstructed pions, kaons and protons.

EPD: The EPD [159] is a dedicated event-plane and centrality detector placed in the forward rapidity region $2 < | \eta | < 4$. With segmentations in both radial and azimuthal directions, the detector will provide precise measurements of both the collision centrality and the event plane. As shown in Fig. 21, the proposed EPD configurations with 12 or 30 ϕ-segmentations are both very close to the optimal case. Additionally, the EPD will be a good trigger detector for collisions at lower beam energies.

4. Summary

The BES-I program at STAR had the following goals: (a) to carry out a search for threshold energies for the signatures of QGP already established at $\sqrt{s_{NN}} = 200$ GeV, corroborating the QGP discovery at RHIC and the LHC; (b) to search for signatures of a first-order phase transition; and (c) to search for a critical point at high μ_B. Toward achieving these goals,

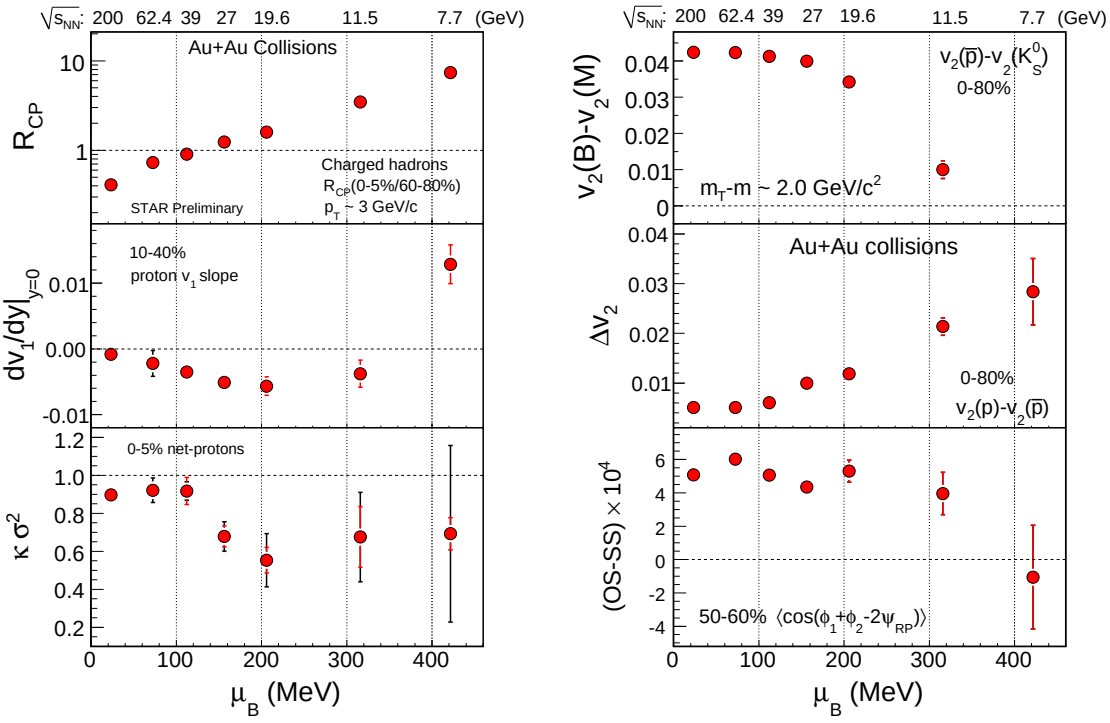

Figure 22. A summary of selected results from the Au+Au collisions in the BES-I program at RHIC as a function of baryon chemical potential. The left panel shows the midrapidity results for the nuclear modification factor for $p_{\rm T} \sim 3$ GeV/c for charged hadrons, the slope of directed flow of protons for 10-40% centrality, and $\kappa\sigma^2$ for net-protons for 0-5% centrality. The right panel shows results for the difference in baryon and meson v_2 at $m_T - m = 2$ GeV/c^2 for minimum-bias collisions, the difference between v_2 of protons and antiprotons for minimum-bias collisions, and the difference between opposite-sign and same-sign charge correlations with respect to the reaction plane for 50-60% centrality. Note that the connection to μ_B is not exact, as μ_B assignment at a given collision energy is dependent on the centrality, and the various analyses have different centrality selections.

Au+Au data were collected by STAR in 2010 and 2011 at 6 energies ($\sqrt{s_{NN}}$ = 7.7, 11.5, 19.6, 27, 39, and 62.4 GeV). Data at the final BES-I energy, 14.5 GeV, were collected in February and March of 2014.

Analysis of the yields of several hadron species ($\pi^{\pm}$, $K^{\pm}$, K^0_S, p, $\overline{p}$, ϕ, Λ, $\overline{\Lambda}$, Ξ, $\overline{\Xi}$, Ω, and $\overline{\Omega}$) suggest that the RHIC BES-I program covered a μ_B range from 20 MeV to about 420 MeV in the QCD phase diagram. Lattice-based QCD calculations indicate that this μ_B range could capture key phase features like the critical point and the region of the first-order phase transition.

A summary of several interesting observations reported here is presented in Fig. 22. All observables exhibit interesting trends as a function of μ_B as the beam energy is changed from 7.7 GeV to 200 GeV. The nuclear modification factor (R_{CP}) for charged hadrons in 0-5% central Au+Au collisions at $p_{\rm T} \sim 3$ GeV/c changes from below unity at μ_B = 20 MeV ($\sqrt{s_{NN}}$ = 200 GeV) to above unity for μ_B = 155 MeV ($\sqrt{s_{NN}}$ = 27 GeV). The slope of the directed flow of protons (dv_1/dy) in mid-central collisions (10-40% centrality) at midrapidity shows

a clear non-monotonic variation with respect to μ_B ($\sqrt{s_{NN}}$). The minimum value of dv_1/dy lies somewhere above μ_B = 205 MeV ($\sqrt{s_{NN}}$ = 19.6 GeV). This observable, which is driven by the pressure gradients developed in the system, is sensitive to first-order phase transition effects. The $\kappa\sigma^2$ of the net-proton number distribution shows an interesting variation with μ_B ($\sqrt{s_{NN}}$). Higher statistics data sets in BES Phase-II will clarify whether the trend will follow a non-monotonic variation with a minimum between μ_B = 155 to 315 MeV ($\sqrt{s_{NN}}$ = 27 to 11.5 GeV) as observed for the proton dv_1/dy or a monotonic variation with μ_B ($\sqrt{s_{NN}}$). The right panel of Fig. 22 shows that the difference in the v_2 of baryons and mesons in minimum-bias Au+Au collisions at m_T - $m \sim 2$ GeV/c^2 decreases with increasing μ_B (decrease in $\sqrt{s_{NN}}$). This difference starts to decrease after μ_B = 155 MeV ($\sqrt{s_{NN}}$ = 27 GeV). The existence of a difference between the v_2 of baryons and meson at intermediate p_{T} is the key to the experimental observation of NCQ scaling and the observation of partonic collectivity at top RHIC energy. It is also observed that the difference in v_2 between baryons and antibaryons (shown for protons and antiprotons in minimum-bias Au+Au collisions at midrapidity in Fig. 22) starts to increases with μ_B (decreases with $\sqrt{s_{NN}}$). Comparison to model calculations suggests that these observations are consistent with the finding that hadronic interactions dominate at lower beam energies. Finally, the difference in the observed signal of dynamical charge correlations between same-sign and opposite-sign charges for 50-60% central Au+Au collisions at midrapidity as a function of μ_B ($\sqrt{s_{NN}}$) is shown. One of the possible explanations for this difference at top RHIC energy is the Chiral Magnetic Effect. This would imply the formation of a deconfined state of quarks and gluons with chiral symmetry restored. The observed trend towards a vanishing of this difference then could indicate the absence of such a quark-hardon transition in the systems at lower beam energies.

The dilepton invariant mass spectrum has promise for revealing the nature of hadronic structure in the vacuum, and insights into chiral symmetry restoration with increasing temperature and/or total baryon density. The dielectron measurements from BES-I only provide enough statistics for studies in the higher energy range $\sqrt{s_{NN}} \geq 20$ GeV. Model calculations are consistent with results from heavy ion collisions at SPS and at various RHIC energies. These calculations indicate that the observed excess yields in the low-mass range could be attributed to rho-meson broadening, driven by the total baryon density in the medium, while the thermal radiation from the partonic phase dominates the intermediate-mass range. While the program at BES Phase-II is designed to study the beam energy dependence of the excess yields in the LMR under high baryon density, the programs at RHIC at higher energies and at LHC will untangle thermal radiation and open heavy-flavor contributions in the IMR. These efforts provide a unique opportunity to validate the scenario where increasing baryon density and/or temperature could lead to chiral symmetry restoration in high-energy nuclear collisions.

The data from BES-I have allowed significant progress to be made toward the goals that had been established at the outset of this program. There is a clear indication that hadronic interactions dominate at the lower BES energies and several observables associated with the formation of a partonic phase at top RHIC energy have been turned-off. These findings corroborate the establishment of QGP at the top RHIC energy. The BES-I program, with

limited event statistics, has made important measurements towards critical point and first-order phase transition physics. This provides compelling reasons for high event statistics in a second phase of the program. These results from the BES-I have allowed us to focus the proposed BES Phase-II on the most crucial energy range from 7.7 to 20 GeV. The enhanced collider performance via increased luminosity due to electron cooling and longer bunches will allow for higher-precision measurements of the key observables. Furthermore, STAR detector upgrades (iTPC and EPD) will allow more comprehensive and refined measurements. A set of focused, high-precision, refined measurements will allow the BES Phase-II program to fundamentally enhance our understanding of the phase diagram of QCD matter.

Acknowledgements

We would like to thank Drs. Francesco Becattini, Elena Bratkovskaya, Alexei Fedotov, Sourendu Gupta, Frithjof Karsch, Cheming Ko, Volker Koch, Olena Linnyk, Jinfeng Liao, Christoph Montag, Hannah Petersen, Owe Phillpsen, Krishna Rajagopal, Ralf Rapp, Jan Steinheimer, Misha Stephanov, Mukherjee Swagato, Ivan Vitev for their invaluable contributions to this document. We thank the RHIC Operations Group and RCF at BNL, the NERSC Center at LBNL, the KISTI Center in Korea and the Open Science Grid consortium for providing resources and support. This work was supported in part by the Offices of NP and HEP within the U.S. DOE Office of Science, the U.S. NSF, CNRS/IN2P3, FAPESP CNPq of Brazil, Ministry of Ed. and Sci. of the Russian Federation, NNSFC, CAS, MoST and MoE of China, the Korean Research Foundation, GA and MSMT of the Czech Republic, FIAS of Germany, DAE, DST, and CSIR of India, National Science Centre of Poland, National Research Foundation (NRF-2012004024), Ministry of Sci., Ed. and Sports of the Rep. of Croatia, and RosAtom of Russia.

References

[1] E. Laermann and O. Philipsen, Ann. Rev. Nucl. Part. Sci. **53** (2003) 163.
[2] K. Fukushima and T. Hatsuda, Rept. Prog. Phys. **74** (2011) 014001.
[3] J. C. Collins and M. J. Perry, Phys. Rev. Lett. **34** (1975) 1353.
[4] E. V. Shuryak, Phys. Rept. **61** (1980) 71.
[5] Y. Aoki, Z. Fodor, S. D. Katz and K. K. Szabo, Phys. Lett. B **643** (2006) 46.
[6] Y. Aoki, S. Borsanyi, S. Durr, Z. Fodor, S. D. Katz, S. Krieg and K. K. Szabo, JHEP **0906** (2009) 088.
[7] S. Borsanyi *et al.*, [Wuppertal-Budapest Collaboration], JHEP **1009** (2010) 073.
[8] A. Bazavov *et al.*, Phys. Rev. D **85** (2012) 054503.
[9] Y. Aoki, G. Endrodi, Z. Fodor, S. D. Katz and K. K. Szabo, Nature, **443** (2006) 675.
[10] S. Ejiri, Phys. Rev. D **78** (2008) 074507.
[11] E. S. Bowman and J. I. Kapusta, Phys. Rev. C **79** (2009) 015202.
[12] M. A. Stephanov, Prog. Theor. Phys. Suppl. **153** (2004) 139; Int. J. Mod. Phys. A **20** (2005) 4387.
[13] C. Alt *et al.*, [NA49 Collaboration], Phys. Rev. C **77** (2008) 024903.
[14] B. I. Abelev *et al.*, [STAR Collaboration], STAR Internal Note - SN0493, 2009.
[15] B. I. Abelev *et al.*, [STAR Collaboration], Phys. Rev. C **81** (2010) 024911.
[16] J. Cleymans, H. Oeschler, K. Redlich and S. Wheaton, Phys. Rev. C **73** (2006) 034905.
[17] P. Braun-Munzinger and J. Stachel, Nature, **448** (2007) 302.

[18] B. I. Abelev *et al.*, [STAR Collaboration], Phys. Rev. C **79** (2009) 034909.
[19] S. Wheaton and J. Cleymans, Comput. Phys. Commun. **180** (2009) 84.
[20] A. Andronic *et al.*, Nucl. Phys. A**834**, (2010) 237.
[21] A. Andronic, P. Braun-Munzinger and J. Stachel, Nucl. Phys. A **772** (2006) 167.
[22] L. Kumar, [STAR Collaboration], Nucl. Phys. A **904, 905** (2013), 256c.
[23] S. Das, [STAR Collaboration], arXiv:1402.0255.
[24] F. Becattini, *et al.*, Phys. Rev. Lett. **111** (2013) 082302.
[25] S. Chatterjee, R. M. Godbole and S. Gupta, Phys. Lett. B **727** (2013) 554.
[26] S. Borsanyi, *et al.*, Phys. Rev. Lett. **111** (2013) 062005.
[27] A. Bazavov, *et al.*, Phys. Rev. Lett. **109** (2012) 192302.
[28] R. V. Gavai and S. Gupta, Phys. Lett. B **696** (2011) 459.
[29] S. Gupta, X. Luo, B. Mohanty, H. G. Ritter and N. Xu, Science, **332** (2011) 1525.
[30] S. Datta, R. V. Gavai and S. Gupta, Nucl. Phys. A **904-905** (2013) 883c.
[31] Z. Fodor and S. D. Katz, JHEP **0404** (2004) 050.
[32] E. Schnedermann, J. Sollfrank and U. W. Heinz, Phys. Rev. C **48** (1993) 2462.
[33] B. Abelev *et al.*, [ALICE Collaboration], Phys. Rev. C **88** (2013) 044910.
[34] J. Adams *et al.* [STAR Collaboration], Nucl. Phys. A **757**, 102 (2005).
[35] M. A. Stephanov, Phys. Rev. Lett. **102**, 032301 (2009).
[36] M. A. Stephanov, Phys. Rev. Lett. **107**, 052301 (2011).
[37] M. Asakawa, S. Ejiri and M. Kitazawa, Phys. Rev. Lett. **103**, 262301 (2009).
[38] M. Cheng *et al.*, Phys. Rev. D **79**, 074505 (2009).
[39] M. M. Aggarwal, *et al.* , [STAR Collaboration], Phys. Rev. Lett. **105** (2010) 022302
[40] L. Adamczyk, *et al.*, [STAR Collaboration], Phys. Rev. Lett. **112** (2014) 032302.
[41] P. Garg, *et al.*, Phys. Lett. B **726** (2013) 691.
[42] L. Adamczyk, *et al.*, [STAR Collaboration], arXiv:1402.1558.
[43] X. Luo, J. Xu, B. Mohanty and N. Xu, J. Phys. G **40** (2013) 105104.
[44] S. A. Bass, *et al.*, Prog. Part. Nucl. Phys. **41** (1998) 255.
[45] M. Bleicher, *et al.*, J. Phys. G **25** (1999) 1859.
[46] B. Schaefer and J. Wambach, Phys.Rev. D **75** (2007) 085015.
[47] D. H. Rischke, Y. Pursun, J. A. Maruhn, H. Stöcker and W. Greiner, Heavy Ion Phys. **1** (1995) 309.
[48] J. Brachmann, *et al.*, Phys. Rev. C **61** (2000) 024909.
[49] H. Stöcker, Nucl. Phys. A **750** (2005) 121.
[50] A. M. Poskanzer and S. A. Voloshin, Phys. Rev. C **58** (1998) 1671.
[51] L. Van Hove, Phys. Lett. B **118** (1982) 138.
[52] H. Petersen, J. Steinheimer, G. Burau, M. Bleicher and H. Stöcker, Phys. Rev. C **78** (2008) 044901.
[53] J. Steinheimer, J. Auvinen, H. Petersen, M. Bleicher and H. Stöcker, arXiv:1402.7236.
[54] L. Adamczyk, *et al.*, [STAR Collaboration], arXiv:1401.3043.
[55] M. Isse, A. Ohnishi, N. Otuka, P. K. Sahu and Y. Nara, Phys. Rev. C **72** (2005) 064908.
[56] L. Ahle, *et al.*, [E866 and E917 Collaborations], Phys. Lett. B **476** (2000) 1.
[57] L. Ahle, *et al.*, [E866 and E917 Collaborations], Phys. Lett. B **490** (2000) 53.
[58] L. Ahle, *et al.*, [E802 Collaboration], Phys. Rev. C **57** (1998) 466.
[59] L. Ahle, *et al.*, [E-802 and E-866 Collaborations], Phys. Rev. C **60** (1999) 044904
[60] J. L. Klay, *et al.*, [E895 Collaboration], Phys. Rev. Lett. **88** (2002) 102301.
[61] J. Barrette, *et al.*, [E877 Collaboration], Phys. Rev. C **62** (2000) 024901.
[62] S. V. Afanasiev, *et al.*, [NA49 Collaboration], Phys. Rev. C **66** (2002) 054902.
[63] E. O'Brien, [PHENIX Collaboration], Nucl. Phys. A **904, 905**, (2013) 264c.
[64] K. Adcox, *et al.*, [PHENIX Collaboration], Nucl. Phys. A **757**, 184 (2005).
[65] M. Gyulassy and L. McLerran, Nucl. Phys. A **750**, 30 (2005).
[66] K. H. Ackermann, *et al.*, [STAR Collaboration], Phys. Rev. Lett. **86** (2001) 402.
[67] C. Adler, *et al.*, [STAR Collaboration], Phys. Rev. Lett. **87** (2001) 182301.
[68] J. Adams, *et al.*, [STAR Collaboration], Phys. Rev. Lett. **92** (2004) 052302.

[69] S. S. Adler, *et al.*, [PHENIX Collaboration], Phys. Rev. Lett. **91** (2003) 182301.
[70] J. Adams, *et al.*, [STAR Collaboration], Phys. Rev. Lett. **91** (2003) 172302.
[71] J. Adams *et al.*, [STAR Collaboration], Phys. Rev. Lett. **91** (2003) 072304.
[72] K. Adcox *et al.*, [PHENIX Collaboration], Phys. Rev. Lett. **88** (2002) 022301.
[73] S. S. Adler *et al.*, [PHENIX Collaboration], Phys. Rev. Lett. **91** (2003) 072301.
[74] B. I. Abelev *et al.*, [STAR Collaboration], Phys. Rev. Lett. **103** (2009) 251601.
[75] B. I. Abelev *et al.*, [STAR Collaboration], Phys. Rev. C **81** (2010) 054908.
[76] B. B. Back *et al.*, [PHOBOS Collaboration], Phys. Rev. C **72** (2005) 051901
[77] B. B. Back *et al.*, [PHOBOS Collaboration], Phys. Rev. Lett. **94** (2005) 122303
[78] J. Adams *et al.*, [STAR Collaboration], Phys. Rev. Lett. **93** (2004) 252301.
[79] S. S. Adler *et al.* , [PHENIX Collaboration], Phys. Rev. Lett. **94** (2005) 232302.
[80] B. I. Abelev *et al.*, [STAR Collaboration], Phys. Rev. Lett. **99** (2007) 112301.
[81] S. K. Tiwari, P. K. Srivastava and C. P. Singh, Phys. Rev. C **85** (2012) 014908.
[82] L. Adamczyk *et al.*, [STAR Collaboration], Phys. Rev. Lett. **110** (2013) 142301.
[83] L. Adamczyk *et al.*, [STAR Collaboration], Phys. Rev. C **88** (2013) 014902.
[84] Y. Burnier, D. E. Kharzeev, J. Liao and H. -U. Yee, Phys. Rev. Lett. **107** (2011) 052303.
[85] J. Steinheimer, V. Koch and M. Bleicher, Phys. Rev. C **86** (2012) 044903.
[86] J. Xu, T. Song, C. M. Ko and F. Li, Phys. Rev. Lett. **112** (2014) 012301.
[87] J. Xu, L. -W. Chen, C. M. Ko and Z. -W. Lin, Phys. Rev. C **85** (2012) 041901.
[88] J. C. Dunlop, M. A. Lisa and P. Sorensen, Phys. Rev. C **84** (2011) 044914.
[89] C.M. Ko, private communications, December, 2013.
[90] D. Molnar and S. A. Voloshin, Phys. Rev. Lett. **91** (2003) 092301.
[91] V. Greco, C. M. Ko and P. Levai, Phys. Rev. C **68** (2003) 034904.
[92] R. J. Fries, B. Muller, C. Nonaka and S. A. Bass, Phys. Rev. C **68** (2003) 044902.
[93] X. Gong, [PHENIX Collaboration], J. Phys. G: Nucl. Part. Phys. **38**, (2011) 124146.
[94] B. Mohanty and N. Xu, J. Phys. G **36** (2009) 064022.
[95] M. Nasim, B. Mohanty and N. Xu, Phys. Rev. C **87** (2013) 014903.
[96] B. I. Abelev *et al.*, [STAR Collaboration], Phys. Lett. B **673** (2009) 183.
[97] Z. -W. Lin and C. M. Ko, Phys. Rev. C **65** (2002) 034904.
[98] Z. -W. Lin, C. M. Ko, B. -A. Li, B. Zhang and S. Pal, Phys. Rev. C **72** (2005) 064901.
[99] B. B. Back *et al.*, [PHOBOS Collaboration], Phys. Rev. Lett. **91** (2003) 072302.
[100] I. Arsene *et al.*, [BRAHMS Collaboration], Phys. Rev. Lett. **91** (2003) 072305.
[101] X. -N. Wang and M. Gyulassy, Phys. Rev. Lett. **68** (1992) 1480.
[102] I. Vitev and M. Gyulassy, Phys. Rev. Lett. **89** (2002) 252301.
[103] M. Gyulassy, P. Levai and I. Vitev, Phys. Rev. Lett. **85** (2000) 5535.
[104] X. -N. Wang, Phys. Rev. C **70** (2004) 031901.
[105] M.L. Miller, K. Reygers, S. J. Sanders and P. Steinberg, Ann. Rev. Nucl. Part. Sci. **57** (2007) 205.
[106] N. Novitzky, [PHENIX Collaboration], J. Phys. G: Nucl. Part. Phys. **38**, (2011) 124149.
[107] M. Gyulassy and X. -N. Wang, Comput. Phys. Commun. **83** (1994) 307.
[108] B. -W. Zhang, E. Wang and X. -N. Wang, Phys. Rev. Lett. **93** (2004) 072301.
[109] S. Wicks, W. Horowitz, M. Djordjevic and M. Gyulassy, Nucl. Phys. A **783** (2007) 493.
[110] I. Vitev, private communication, (2014).
[111] R. B. Neufeld, I. Vitev and B. -W. Zhang, Phys. Lett. B **704** (2011) 590.
[112] I. Vitev, Phys. Rev. C **75** (2007) 064906.
[113] G. Ovanesyan and I. Vitev, JHEP **1106** (2011) 080.
[114] G. Ovanesyan and I. Vitev, Phys. Lett. B **706** (2012) 371.
[115] P. Huovinen and H. Petersen, Eur. Phys. J. A **48** (2012) 171.
[116] J. Steinheimer and M. Bleicher, Phys. Rev. C **84** (2011) 024905.
[117] C. Nonaka and S. A. Bass, Nucl. Phys. A **774** (2006) 873.
[118] J. Steinheimer, S. Schramm and H. Stocker, Phys. Rev. C **84** (2011) 045208.
[119] D. Kharzeev, R. D. Pisarski and M. H. G. Tytgat, Phys. Rev. Lett. **81** (1998) 512.

[120] D. Kharzeev, Phys. Lett. B **633** (2006) 260.
[121] D. E. Kharzeev, L. D. McLerran and H. J. Warringa, Nucl. Phys. A **803** (2008) 227.
[122] K. Fukushima, D. E. Kharzeev and H. J. Warringa, Phys. Rev. D **78** (2008) 074033.
[123] L. Adamczyk *et al.*, [STAR Collaboration], arXiv:1302.3802.
[124] B. Abelev *et al.*, [ALICE Collaboration], Phys. Rev. Lett. **110** (2013) 012301.
[125] S. A. Voloshin, Phys. Rev. C **70** (2004) 057901.
[126] S. Schlichting and S. Pratt, Phys. Rev. C **83** (2011) 014913.
[127] A. Bzdak, V. Koch and J. Liao, Phys. Rev. C **83** (2011) 014905.
[128] A. Bzdak, V. Koch and J. Liao, Lect. Notes Phys. **871** (2013) 503.
[129] R. Rapp and J. Wambach, Adv. Nucl. Phys. **25** (2000) 1.
[130] J. Alam, S. Sarkar, P. Roy, T. Hatsuda and B. Sinha, Annals Phys. **286** (2001) 159.
[131] G. E. Brown and M. Rho, Phys. Rept. **269** (1996) 333.
[132] D. Adamova *et al.*, [CERES/NA45 Collaboration], Phys. Rev. Lett. **91** (2003) 042301.
[133] R. Arnaldi *et al.*, [NA60 Collaboration], Phys. Rev. Lett. **96** (2006) 162302.
[134] H. van Hees and R. Rapp, Phys. Rev. Lett. **97** (2006) 102301.
[135] J. Ruppert, C. Gale, T. Renk, P. Lichard and J. I. Kapusta, Phys. Rev. Lett. **100** (2008) 162301.
[136] K. Dusling, D. Teaney and I. Zahed, Phys. Rev. C **75** (2007) 024908.
[137] O. Linnyk, E. L. Bratkovskaya, V. Ozvenchuk, W. Cassing and C. M. Ko, Phys. Rev. C **84** (2011) 054917.
[138] A. Adare *et al.*, [PHENIX Collaboration], Phys. Rev. C **81** (2010) 034911.
[139] L. Adamczyk *et al.*, [STAR Collaboration], arXiv:1312.7397.
[140] R. Rapp, Phys. Rev. C **63** (2001) 054907; Phys. Rev. A **83** (2011) 043833.
[141] R. Rapp, J. Wambach and H. van Hees, arXiv:0901.3289.
[142] B. Friman *et al.*, (Eds.), *The CBM Physics Book*, Lect. Notes Phys. 814 [DOI: 10.1007/978-3-462-13293-3]
[143] D. Adamova *et al.*, [CERES/NA45 Collaboration], Phys. Lett. B **666** (2008) 425.
[144] O. Linnyk, private communication; W. Cassing, E.L. Bratkovskaya, S. Juchem, Nucl. Phys. A **674** (2000) 249.
[145] R. Rapp, Adv. High Energy Phys. **2013** (2013) 148253.
[146] H. van Hees and R. Rapp, Nucl. Phys. A **806** (2008) 339.
[147] M. Lisa, U. Heinz, U. Weidemann, Phys. Lett. B **489** (2000) 287.
[148] E. Mount, G. Graef, M. Mitrovski, M. Bleicher, M.A. Lisa, Phys. Rev. C **84** (2011) 014908.
[149] G. Graef, M.A. Lisa, M. Bleicher, Phys. Rev. C **89**, (2014) 014903.
[150] L. Adamczyk *et al.*, [STAR Collaboration], arXiv: 1403.4972; C. Anson, [STAR Collaboration], J. Phys. G: Nucl. Part. Phys. **38**, (2011) 124148.
[151] V. Magas, L.P. Csernai, and D. Strottmann, Nucl. Phys. A **712** (2002) 167.
[152] J. Brachmann *et al.*, Phys. Rev. C **61** (2000) 024909.
[153] L.V.Bravina, Phys. Lett. B **344** (1995) 49.
[154] A. Rustamov, Cent. Eur. J. Phys. **10**, (2012) 1267.
[155] I. C. Arsene *et al.*, Phys. Rev. C **75**, (2007) 034902.
[156] J. Randrup, Phys. Rev. C **79**, (2009) 054911.
[157] J. Randrup, Phys. Rev. C **82**, (2010) 034902 .
[158] iTPC upgrade document, (2014): `https://drupal.star.bnl.gov/STAR/upgrade-inner-sectors-time-projection-chamber`
[159] EPD technical document, (2014): `https://drupal.star.bnl.gov/STAR/system/files/`
[160] eTOF technical document, (2014): `https://drupal.star.bnl.gov/STAR/system/files/`